Composite Structures

Experimental and analytical investigation of PBO FRCM-concrete bond behavior using direct and indirect test set-ups

--Manuscript Draft--

Manuscript Number:	COMSTR-D-20-02003R1
Article Type:	Full Length Article
Keywords:	Bond; FRCM; direct shear test; modified beam test; Analytical model
Corresponding Author:	Tommaso D'Antino Politecnico di Milano Milan, Italy
First Author:	Angelo Savio Calabrese
Order of Authors:	Angelo Savio Calabrese
	Tommaso D'Antino
	Pierluigi Colombi
Abstract:	Externally bonded reinforcement (EBR) represents an effective solution to strengthen existing reinforced concrete (RC) members. EBR comprising fiber-reinforced cementitious matrix (FRCM) has been increasingly adopted due to some advantages with respect to the more diffused fiber-reinforced polymer (FRP). Externally bonded FRCM often reported debonding failure at the matrix-fiber interface. In the literature, the matrix-fiber bond behavior was studied using mostly single- and double-lap direct shear (DS) tests. An alternative is represented by modified beam (MB) test set-ups. In this paper, a MB test set-up is adopted to study the effect of flexural deflection on the bond behavior of a polyparaphenylene benzobisoxazole (PBO) FRCM composite bonded to a concrete substrate. Two different MB test layouts are investigated and the results obtained are analyzed and compared with those of corresponding DS tests with the same PBO FRCM. Then, an analytical model able to describe the results of both DS and MB tests accounting for the presence of stresses normal to the matrix-fiber interface is proposed. The experimental results and analysis presented in this paper help to clarify the influence of the test set-up on the bond behavior of FRCM composites, which represents a key parameter for the design of FRCM EBR.
Suggested Reviewers:	Francesco Focacci Associate Professor, University eCampus francesco.focacci@uniecampus.it Prof. Focacci has been studying composites materials and their bond behaviour for several years. He is involved in international scientific committees on this topic and published numerous contributions.
	Lesley Sneed Professor, Missouri S&T: Missouri University of Science and Technology sneedlh@mst.edu Prof Sneed is an expert on organic- and inorganic-matrix composites. She is a member of ACI 549 and provided numerous contributions on the study of composite bond behaviour.
	Paraskevi Askouni Assistant Professor, University of Patras: Panepistemio Patron askounip@upatras.gr Dr Askouni has been active in inorganic-matrix composites in the last years. Her work focused on the composite bond behaviour both from the experimental and analytical point of view.
Response to Reviewers:	See attached Response to Reviewers file.

**Dipartimento di Architettura, Ingegneria delle Costruzioni
e Ambiente Costruito**

POLITECNICO DI MILANO

Prof. A. J. M. Ferreira, PhD
Composite Structures

Milan, January 28, 2021

Dear Prof. Ferreira:

I am pleased to submit the attached revised manuscript for consideration for publication in Composite Structures. In this paper, the bond behavior of an inorganic-matrix composites comprising polyparaphenylene benzobisoxazole (PBO) fibers is investigated using direct shear and modified beam tests. The results obtained by the experimental campaign are carefully presented and discussed to shed light on the influence of the test set-ups on the parameters measured. Then, based on the results obtained, an analytical approach based on the solution of the bond differential equation is proposed. The analytical approach is able to describe both the load response of direct shear tests and of modified beam tests using the concept of snubbing friction.
We have provided the responses to the Reviewers' Comments in a separate file and revised the manuscript accordingly.

If there is any further information you need at this time, please let me know. My email and phone number are provided below. Thank-you for your consideration.

Sincerely,

Tommaso D'Antino, Ph.D.
Assistant Professor
Email: tommaso.dantino@polimi.it
Phone: +39 02 2399 4352

Politecnico di Milano
Dipartimento di Architettura, Ingegneria delle Costruzioni
e Ambiente Costruito
Via Ponzio, 31
20133 Milano
02 2399 5404/5406
Fax 02 2399 5195

www.abc.polimi.it
Partita Iva: 04376620151
Codice fiscale: 80057930150

Title: Experimental and analytical investigation of PBO FRCM-concrete bond behavior using direct and indirect test set-ups
Manuscript Number: COMSTR-D-20-02003
Authors: Angelo Savio Calabrese, Tommaso D'Antino, Pierluigi Colombi

The authors would like to thank the editor and the reviewer for their helpful comments. The response to each comment is provided below and a revised copy of the manuscript, in which the revisions were marked in red, is attached to this document.

Reviewer 1

The paper addresses the interesting subject of experimental characterization of PBO-FRCM-EBR composite to substrate binding (polyparaphenylene benzobisoxazole fiber-reinforced cementitious matrix externally bonded reinforcement).
The article is well written and easy to read (except the impressive number of acronyms). It contains some new information compared to similar articles published by the same authors (some additional experimental results concerning FRCM binding to concrete, and the analytical part).
The authors appreciate the reviewer's acknowledgment regarding the importance of the subject, the quality of the manuscript, and the relevance of the experimental results.

Some typos:

- In Table 1 and 2, the residual stress σ_0 ,f should be in [MPa], not in [mm]
  The typo was corrected, thank-you.
- Line 382: there is an extra "by"
  The typo was corrected, thank-you.
- Eq. (5) and Eq. (11): this should be σ with hat (^) instead of σ. By the way, it is not clever to choose the notation σ (even with a hat) for a dimensionless quantity. It can be confusing, especially if you forget the hat. f(alpha) is good, why not use it?
  Thank-you for your comment. The missing "hat" was due to conversion from word to pdf, which we could not fix (there was no way to avoid it apparently). Anyway, following the Reviewer's suggestion, sigma(hat) was replaced by rho(alfa).
- Eq. (5): specify the μ symbol right after, it is only given at line 476, much further on.
  The sentence "and μ is the snubbing friction coefficient [46]" was added to line 392 according to the Reviewer's comment.

General comments:

The authors should add some information or comments on the generality of their f(alpha) formula to correct the influence of normal stresses (identified on some tests): does it depend on the geometry of the reinforcement, the materials, ... ? If yes, does it not discredit the MB test, since in this case it is necessary to systematically perform DS tests to calibrate this function f(alpha)?
The Reviewer raised a key point. The MB test is more complex than a shear test and provide results that are affected by the presence of a stress component normal to the matrix-fiber interface. However, the MB test may be useful when the FRCM-strengthened members is subjected to non-pure Mode-II loading condition. In these cases, the MB test would provide values of fiber stress close to those of the FRCM applied to the strengthened member. To clarify this point, the following sentence was added to the

introduction (lines 79-83): “Accordingly, modified beam tests can be employed to evaluate the load-carrying capacity of FRCM-strengthened members where the composite is subjected to a non-pure Mode-II loading condition [30-33]. In these cases, the MB test would provide values of fiber stress close to those of the FRCM applied to the strengthened member [10]”.

The snubbing coefficient is a property of the FRCM and, if a relationship between direct shear and modified beam tests is sought, can be estimated experimentally with pull-out tests of fiber bundles embedded within matrix prisms varying the bonded length and angle of inclination of the pulling force. To clarify this point, the following sentence was added to lines 397-399: “The coefficient μ in Eq. (5) is a property of the specific FRCM composite and can be estimated experimentally with pull-out tests of fiber bundles embedded within matrix prisms varying the bonded length and angle of inclination of the pulling force [46]”.

Experimental and analytical investigation of PBO FRCM-concrete bond behavior using direct and indirect test set-ups

Angelo Savio Calabrese, Tommaso D'Antino*, Pierluigi Colombi

Politecnico Milano 1863, Department of Architecture, Built Environment and Construction Engineering, Milan, IT

Abstract

Externally bonded reinforcement (EBR) represents an effective solution to strengthen existing reinforced concrete (RC) members. EBR comprising fiber-reinforced cementitious matrix (FRCM) has been increasingly adopted due to some advantages with respect to the more diffused fiber-reinforced polymer (FRP). Externally bonded FRCM often reported debonding failure at the matrix-fiber interface. In the literature, the matrix-fiber bond behavior was studied using mostly single- and double-lap direct shear (DS) tests. An alternative is represented by modified beam (MB) test set-ups. In this paper, a MB test set-up is adopted to study the effect of flexural deflection on the bond behavior of a polyparaphenylene benzobisoxazole (PBO) FRCM composite bonded to a concrete substrate. Two different MB test layouts are investigated and the results obtained are analyzed and compared with those of corresponding DS tests with the same PBO FRCM. Then, an analytical model able to describe the results of both DS and MB tests accounting for the presence of stresses normal to the matrix-fiber interface is proposed. The experimental results and analysis presented in this paper help to clarify the influence of the test set-up on the bond behavior of FRCM composites, which represents a key parameter for the design of FRCM EBR.

Keywords: bond, FRCM, direct shear test, modified beam test, analytical model.

*Corresponding author: tommaso.dantino@polimi.it

1 Introduction

In the last few years, fiber-reinforced cementitious matrix (FRCM) composites have been attracting increasing interest as externally bonded reinforcement (EBR) of existing masonry and reinforced concrete (RC) structures. FRCMs are comprised of inorganic matrices (typically cement- or lime-based matrices) reinforced with one or multiple layers of high-strength open-mesh fiber (usually carbon, glass, basalt, or polyparaphenylene benzobisoxazole, PBO) textiles. Several studies were conducted to investigate the contribution of various FRCM composites to the load-carrying capacity of different structural members. These studies showed that FRCM composites are effective in increasing the axial [1,2], bending [3,4], and shear [5,6] capacity of RC members, as well as the in-plane [7] and out-of-plane capacity of masonry walls [8,9] and the capacity of masonry arches [10]. Furthermore, the use of inorganic matrices is responsible for some advantages of FRCMs over organic-matrix fiber-reinforced composites, such as the good thermal and vapor compatibility with inorganic substrates [11], good behavior at relatively high temperatures [12], and partial reversibility of the application [13].

However, due to the dimension of their components, inorganic binders can hardly impregnate all fiber filaments of bare (i.e. not impregnated) textiles, which leads to premature debonding at the matrix-fiber interface and, in some cases, to a textile telescopic failure [14]. FRCM debonding failure, which is typically associated with stress levels significantly lower than the tensile strength of corresponding FRCM coupons [15], may occur at one of the interfaces present in the strengthened member as a function of the substrate and composite layout and properties [3]. For applications involving more than two textile layers, debonding was reported at the composite-substrate interface without damage of the substrate [3]. For inorganic-matrix composites including unidirectional steel cord textiles, referred to as steel reinforced grout (SRG) in the literature, debonding between the matrix layers embedding the textile was often reported [16].

Due to the occurrence of debonding failures, the FRCM bond capacity represents a fundamental parameter for the estimation of the composite contribution to the strengthened member load-carrying capacity, as recognized by the recently-released Italian guidelines for design and construction of EBR FRCM reinforcements systems for strengthening existing structures [17].

In the literature, different set-ups were adopted to investigate the bond capacity of externally bonded reinforcement of concrete and masonry members. The single- and double-lap direct shear test set-ups are the most diffused [15,18,19]. In these tests, the interface is generally assumed to be subjected to a pure fracture mechanics Mode-II loading condition, although stress components normal to the interface can arise due to the eccentricity between the forces applied to the bonded strips and substrate [20]. The presence of interface normal stress components that tend to open the interface crack, which is thus subjected to a mixed mode Mode-I/II loading condition, was observed at the ends of fiber-reinforced polymer (FRP) strengthened RC beams and was postulated to be responsible of the plate end (PE) debonding failure [21]. However, normal stresses that tend to push the composite toward the interface were observed away from the composite ends in FRP strengthened RC beams. These stresses were assumed to increase the interface bond capacity depending on the member cross-section curvature [22] and were accounted for in the formulation provided by fib bulletin 90 [23] to compute the composite maximum force associated with intermediate-crack (IC) induced debonding failure. A beneficial effect of stresses normal to the interface where debonding occurs was also observed in FRP- and FRCM-strengthened curved masonry members with composite strips externally bonded on the member convex face [24,25].

Experimental direct shear tests were carried out to investigate the effect of interface normal stress components on EB FRP, FRCM, and SRG composites [26–28]. These studies showed that interface normal stresses arise along the interface where debonding occurs as an effect of the member curvature and confirmed that they can increase the composite bond capacity in the case of convex substrates, whereas they induce premature debonding in the case of concave substrates [29]. Recently, small-scale bending tests were adopted to study the interaction between interface shear and normal stresses

in FRCM-masonry joints [24,30]. Namely, modified beam tests, where two masonry prisms were connected by a cylindrical hinge at the midspan top side and by a composite strip on the prims bottom face, showed that the member deflection induced a normal stress component that increased the specimen maximum force, although inducing eventual rupture of the textile [31]. Accordingly, modified beam tests can be employed to evaluate the load-carrying capacity of FRCM-strengthened members where the composite is subjected to a non-pure Mode-II loading condition [30–33]. In these cases, the MB test would provide values of fiber stress close to those of the FRCM applied to the strengthened member [10].

Several analytical and numerical models were proposed to reproduce the bond behavior of externally bonded composites subjected to either a pure Mode-II or to a mixed Mode-I/II loading conditions. Typically, a continuous or multi-linear interface shear stress τ - slip s relationship, also referred to as the interface cohesive material law (CML), was employed to model the bond behavior under a pure Mode-II condition. When interface normal stresses are present, interface normal stress σ – crack opening w relationships were also considered [20,32–36].

In this paper, the effect of the normal stress component at the matrix-fiber interface of a polyparaphenylene benzo-bisoxazole (PBO) composite applied onto a concrete substrate is studied. The results of eight single-lap direct shear tests of PBO FRCM-concrete joints and of six modified beam tests with the same PBO FRCM and concrete substrates are presented. The composite bonded length and width were kept constant in the two set-ups. Two different layouts of the composite strip were considered in the modified beam tests to investigate the influence of the matrix at the specimen midspan on the behavior observed. Then, the experimental results obtained are modeled using an analytical approach previously adopted by the authors to model the matrix-fiber bond behavior in PBO FRCM pull-out tests [37]. This approach is here extended to the case of modified beam tests to account for the effect of the normal stress component. The experimental and analytical results described in this paper help shedding light on the complex bond behavior of FRCM composites when shear and normal stresses are present in the composite-substrate joint.

2 Materials

A PBO FRCM composite, comprising one layer of an unbalanced textile and two 5 mm thick layers of a cement-based matrix, was used in this study. The textile had longitudinal and transversal bundles spaced at 10 and 17.5 mm on center, respectively. The equivalent thickness of the textile in longitudinal direction, which was the direction parallel to the composite strip longitudinal axes, was t_f=0.046 mm. The average tensile strength and elastic modulus of the PBO textile in longitudinal direction were obtained in [38] by tensile tests of PBO textile strips with different widths and were equal to 3015 MPa (CoV=6.8%) and 206 GPa (CoV=6.5%), respectively. The cement-based matrix compressive and splitting tensile strength were measured by tests on matrix cylinders with diameter 50 mm and height 100 mm and were equal to 28.4 MPa (CoV=9.2%) and 3.5 MPa (CoV=23.1%), respectively [38].

Two different concrete batches were used for the concrete blocks employed in the modified beam and in the direct shear tests. The blocks employed in all modified beam tests and in the direct shear tests with bonded width b_1=60 mm (see Section 3.2) were characterized by compressive tests on six 150×150×150 mm^3 cubes and by splitting tests on five 100×200 mm^2 cylinders. The average compressive and splitting tensile strengths obtained were 37.9 MPa (CoV=6.02%) and 2.50 MPa (CoV=18.40%), respectively. The blocks employed for the direct shear tests with bonded width b_1=50 mm (see Section 3.2) were characterized by compressive tests on seven 150×150×150 mm^3 cubes, which provided and average compressive strength of 29.4 MPa (CoV=5.41%). The corresponding tensile strength was not measured experimentally.

3 Experimental set-ups

Fourteen tests [8 single-lap direct shear (DS) and 6 modified beam tests (MB)] are considered. Note that 3 MB and 5 DS tests were performed in this experimental campaign, while the remaining 3 MB and 3 DS tests were previously published in [39] and are reported here for comparison. The specimen

dimensions and test set-ups are shown in Figure 1 and are described in the following sections. Both MB and DS tests were performed in displacement control by monotonically increasing the machine stroke at a rate of 0.2 mm/min [40].

3.1 Modified beam test

The MB test specimens were comprised of two concrete prisms connected by a cylindrical hinge at the top side and by a composite strip along the bottom faces (Figure 1a). Two different strip layouts were adopted for these specimens. In the first, named bare-fiber layout, the textile was left bare (i.e. it was not impregnated by the matrix) along 60 mm at the modified beam midspan (Figure 1b), which allowed for a direct measure of the bare fiber-substrate relative displacement at the two loaded ends of the specimen (Figure 1b). In the second layout, named bond-gap layout, the matrix was not bonded to the substrate along 60 mm at the modified beam midspan (Figure 1c). This layout reproduces the composite-substrate bond interruption generally adopted at the loaded end of FRP- and FRCM-concrete direct shear and modified beam tests to prevent the substrate wedge failure [40,41]. For both the bare-fiber and bond-gap layout, the bonded length and width of the strip applied to each concrete prism were L=300 mm and b_1=60 mm (i.e. 6 longitudinal fiber bundles), respectively. A portion of textile was left bare at the strip free ends of specimens with bond-gap layout (Figure 1d) to measure the corresponding bare fiber-substrate relative displacement.

The MB specimens were tested under a 4-point bending configuration. Two cylindrical steel supports were placed at a distance of 900 mm while the load was applied using two steel cylinders placed at a distance of 80 mm from each other and connected to the machine through a spherical hinge. The specimens were equipped with six or eight (depending on the strip layout) linear variable displacement transducers (LVDTs). In bare-fiber specimens, four LVDTs (two on each side of the strip, named LVDT B1, B2, B3, and B4, see Figure 1b) were employed to measure the fiber-substrate relative displacement at the two loaded ends. LVDTs B1-B4 were attached to the concrete substrate and reacted off of aluminum L-shaped plates bonded to the bare fibers immediately outside the matrix

154 at the loaded ends. In bond-gap specimens, two LVDTs (one on each side of the strip, named LVDT
155 G1 and G2, see Figure 1c) attached to the concrete block and reacting off of aluminum L-shaped
156 plates attached to the opposite block were used to measure the relative displacement between blocks.
157 Four LVDTs (two on each block, one on each side of the composite strip, namely, LVDT G3, G4,
158 G5, and G6, see Figure 1d) measured the fiber-substrate relative displacement at the free ends of
159 bond-gap specimens. Finally, in all MB specimens, two LVDTs (one on each side of the specimen,
160 named LVDT V1 and V2, see Figure 1b and c) were used to measure the vertical deflection at
161 midspan.

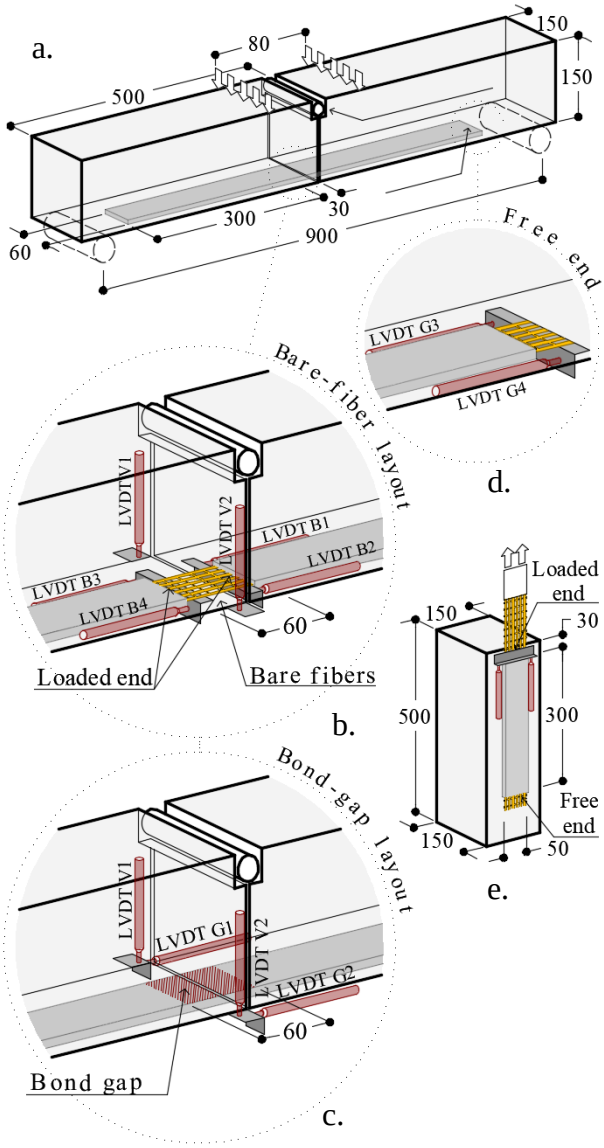

162

163 Figure 1. a) Modified beam test geometry and set-up: b) bare-fiber, c) bond-gap specimen midspan,
164 and d) detail of the free end. e) Direct shear test geometry and set-up (dimensions in mm).

3.2 Direct shear test

The DS test specimens were realized by applying the same PBO FRCM used in the MB test to the lateral surface of a concrete prism with 150×150 mm^2 cross-section and a 500 mm length (Figure 1e). The composite bonded length was L=300 mm, whereas two bonded widths, namely b_1=50 mm (including 5 longitudinal fiber bundles) and b_1=60 mm (including 6 longitudinal fiber bundles), were employed. The composite strip loaded end was placed 30 mm far from the concrete block edge, as usually recommended to avoid substrate wedge failure [40,41]. The matrix thickness was in total equal to 10 mm (5 mm for each layer) as in the MB test specimens. The textile was left bare for approximately 300 mm outside the loaded end and was equipped with two epoxy bonded steel plates at the end to facilitate gripping by the testing machine (Figure 1e). An L-shaped aluminum plate was glued to the bare textile just outside the composite strip at the loaded end. Two LVDTs were attached to the concrete at the loaded end and reacted off of the L-shaped aluminum plate to measure the fiber-concrete relative displacement.

4 Results

Specimens were named following the notation MB_(or DS)_X_Y_(G or B)_n, where MB=modified beam test or DS=direct shear test, X and Y are the bonded length and width (in mm), respectively, G (=bond-gap) or B (=bare-fibers) indicates the strip layout for the MB tests, and n is the specimen number. The specimens are listed in Table 1 and Table 2.

Table 1. Modified beam experimental test results.

Specimen	w [mm]	h [mm]	l_W [mm]	$L^{\dagger}$ [mm]	b_1 [mm]	σ_0^{*} [MPa]	g^{*} [mm]	$\sigma_{0,f}$ [MPa]	g_f [mm]
MB_300_60_B_1				300	60	2220	1.47	199	5.59

Specimen	w [mm]	h [mm]	l_W [mm]	$L^{\dagger}$ [mm]	b_1 [mm]	σ_0^* [MPa]	g^* [mm]	$\sigma_{0,f}$ [MPa]	g_f [mm]
MB_300_60_B_2	410	150	200			2124	2.47	481	5.51
MB_300_60_B_3						2135	1.61	430	5.85
Average ($\bar{\cdot}$)						2159	1.83	370	6.00
CoV	-	-	-	-	-	0.024	0.243	0.406	0.031
Average curve MB_B_avg ($\bar{\cdot}$)						2142	1.32	277	5.55
MB_300_60_G_1						2499	1.89	671	4.59
MB_300_60_G_2	410	150	200	300	60	2514	2.14	283	4.72
MB_300_60_G_3						2617	1.58	434	6.35
Average ($\bar{\cdot}$)						2543	1.87	463	5.22
CoV	-	-	-	-	-	0.025	0.149	0.422	0.188
Average curve MB_G_avg ($\bar{\cdot}$)						2522	1.89	514	5.94

187 †Bonded length of a single block; σ_0^* = peak fiber stress; g^* = global slip at the peak fiber stress; $\sigma_{0,f}$

188 = residual fiber stress, g_f = global slip at the first attainment of the residual fiber stress.

189

190 Table 2. Direct shear experimental test results.

Specimen	L [mm]	b_1 [mm]	σ^* [MPa]	g^* [mm]	σ_f [MPa]	g_f [mm]
DS_300_60_1			2090	0.95	123	5.98
DS_300_60_2	300	60	1673	2.86	319	6.51
DS_300_60_3			1813	2.15	112	6.20
DS_300_50_1			1938	1.39	239	6.92
DS_300_50_2	300	50	2230	0.87	219	7.81
DS_300_50_3			2224	1.22	231	7.03

Specimen	L [mm]	b_1 [mm]	σ^* [MPa]	g^* [mm]	σ_f [MPa]	g_f [mm]
DS_300_50_4			2190	1.64	331	6.94
DS_300_50_5			2148	1.15	269	6.92
Average ($\bar{\cdot}$)			2038	1.53	230	6.79
CoV	-	-	0.102	0.441	0.350	0.083
Average curve DS_avg ($\bar{\cdot}$)			1971	1.15	230	7.15

191 σ^* = peak axial stress; g^* = global slip at the peak axial stress; σ_f = residual axial stress; g_f = global
192 slip at the first attainment of the residual axial stress.
193
194 For all specimens, failure occurred due to debonding of the fiber from the embedding matrix, as
195 previously reported for several different FRCM composites comprising one or two layers of textile
196 [18,42–44]. In the following sections, the load response and bond behavior observed are described
197 and discussed for each set-up considered.
198
199 ***4.1 Modified beam test - Bare-fiber layout***
200 The load response of specimen MB_300_60_B_3, which is representative of the load responses
201 obtained with MB tests with bare-fiber layout, is shown in Figure 2a. For bare-fiber specimens, the
202 global slip g is the average of the displacements measured by the two LVDTs reading at the loaded
203 end of the same concrete block (either LVDT B1 and B2 or B3 and B4, see Figure 1b), whereas the
204 fiber stress σ_0 was computed by enforcing the specimen equilibrium, as shown in Figure 3a [39,45]:
205 $$\sigma_0 = \frac{T}{A} = \frac{Pw + 2Wl_W}{2h\cos\alpha}\frac{1}{A} \quad (1)$$
206 where $T = \sigma_0 A$ is the force in the composite, A is the fiber cross-sectional area ($A=t_f b_1$), α is the
207 specimen rotation angle, P is the load measured by the machine load cell, w is the distance between
208 one of the two loading points and the closest support, W=258 N is the self-weight of the prism

(assumed concentrated in the prism centroid), l_W is the horizontal distance between the prism centroid and the closest support, and h is the vertical distance between the axis of the cylindrical hinge and textile plane (see Table 1). In Figure 2a, the fiber stress σ_0 (or applied load T) is plotted versus the global slip measured at the two loaded ends. The side of the specimen associated with each global slip is named fully debonded side (FDS) or partially debonded side (PDS) depending on the behavior observed during the test [31], as explained in the following.

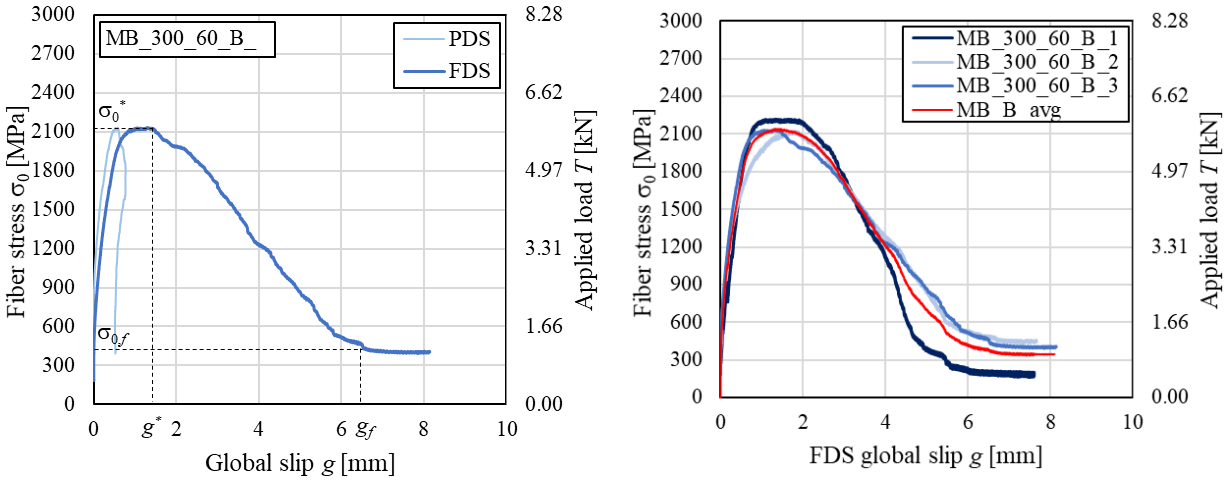

a. b.

Figure 2. Load responses of bare-fiber MB tests: a) specimen MB_300_60_B_3 (g measured at the PDS and FDS) and b) specimens MB_300_60_B_1-3 (g measured at the FDS).

The load responses in Figure 2 showed an initially linear behavior, associated with an almost identical matrix-fiber slip at the two loaded ends (Figure 2a). As the machine stroke was increased, the load response became non-linear due to the presence of micro-cracking at the matrix-fiber interface. At the end of the linear branch, the fiber slip at the loaded end associated with the fully debonded side (FDS) started to increase at a higher rate compared to that at the opposite loaded end, which is associated with the partially debonded side (PDS). With increasing machine stroke, the fiber stress attained the peak value σ_0^* (associated to a global slip g^*), after which the load (stress) response showed a softening branch characterized by increasing values of global slip at the FDS, whereas at

the PDS g remained approximately constant or slightly decreased due to the recovery of the fiber elastic deformation (see Figure 2a and Figure 4c). At the end of the test, the fiber stress attained a constant value, equal to $\sigma_{0,f}$, due to the presence of friction at the matrix-fiber interface [30,37]. For specimen MB_300_60_B_1, $\sigma_{0,f}$ was lower than that of specimens MB_300_60_B_2 and 3 (Figure 2b). This difference was attributed to the rupture of some fiber filaments, which might have been caused by the stress component normal to the fiber textile plane, as previously observed for modified beam tests comprising masonry blocks [31].

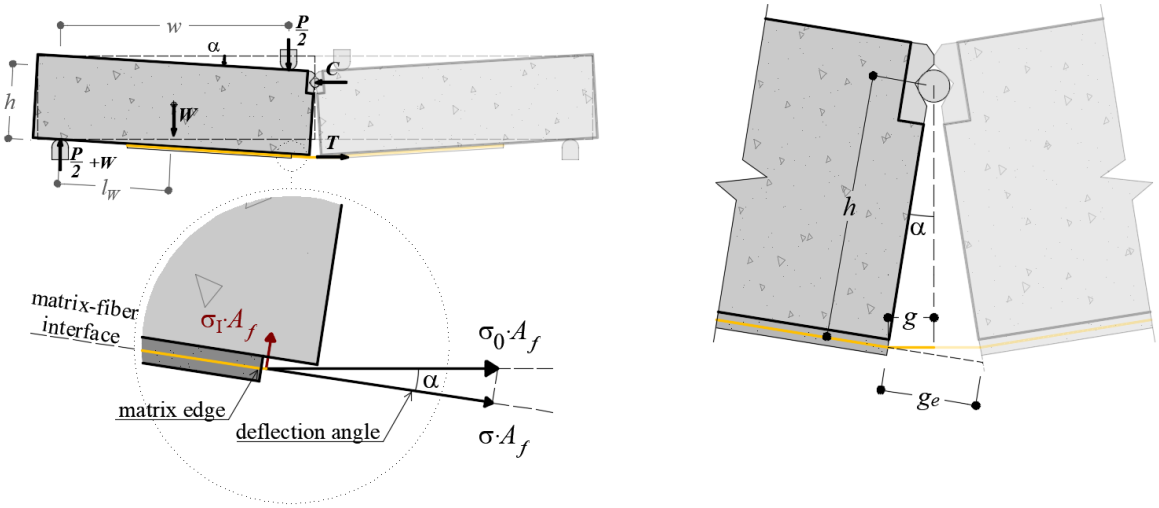

a. b.

Figure 3. a) Free body diagram of the MB test. b) Representation of g_e.

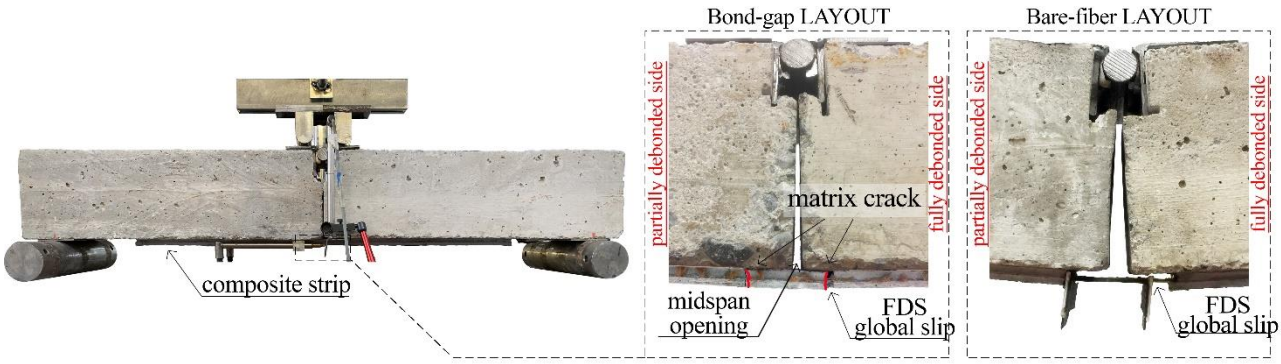

a) b) c)

Figure 4. MB test: a) side view and detail of the midspan for b) bond-gap and c) bare-fiber layouts.

4.2 Modified beam test - Bond-gap layout

Figure 5a shows the σ_0 - g_e response of a representative MB test with bond-gap layout (specimen MB_300_60_G_2), where g_e is the average displacement recorded by LVDT G1 and G2 (see Figure 1c and Figure 3b) and σ_0 is the fiber stress computed by Eq. (1). It should be noted that the displacement g_e is affected by the relative rotation between blocks (Figure 3b) and should not be referred to as the global slip g. The average displacement measured by each couple of LVDTs reading at the free end of each block (either LVDT G3 and G4 or G5 and G6, see Figure 1e) was named free end slip s_F.

The MB tests with bond-gap layout showed an initial linear load response, which was interrupted due to the occurrence of a matrix transversal crack located at one of the two loaded ends (i.e. at the beginning of the bond gap, see Figure 4b). This crack occurred at a fiber stress $\sigma_{0,A}$ of approximately 700 MPa (associated with the displacement $g_{e,A}$, see Figure 5a), which is equivalent to a matrix stress of $\sigma_{m,A}=\sigma_{0,A}A/A_m=3.22$ MPa (where $A_m=50$ mm^2 is the matrix cross-sectional area) that is consistent with the matrix splitting tensile strength measured (3.5 MPa, see Section 2). After the occurrence of the first matrix crack, the slope of the load response decreased significantly and, with increasing the machine stroke, a new matrix crack occurred at the loaded end opposite to that where the first matrix crack occurred (Figure 4b). These two matrix cracks opened at different rates during the test. After the attainment of the peak fiber stress σ_0^*, which was associated with the displacement g_e^* (Figure 5a), only one of the two matrix cracks [located at the fully debonded side (FDS)], continued to open whereas the width of the other remained approximately constant (PDS). This indicates that, as in the case of MB test with bare-fiber layout, the composite strip behavior was not perfectly symmetrical during the test and the matrix-fiber slip increased only in one side of the specimen. The LVDTs reading at the free ends confirmed this observation, since free end matrix-fiber slip s_F was recorded only on the specimen FDS, where the crack whose width increased throughout the entire test was

located. The σ_0 - s_F curve of specimen MB_300_60_G_3 is shown in Figure 5a. The σ_0 - s_F curves of the remaining specimens can be found in [39].

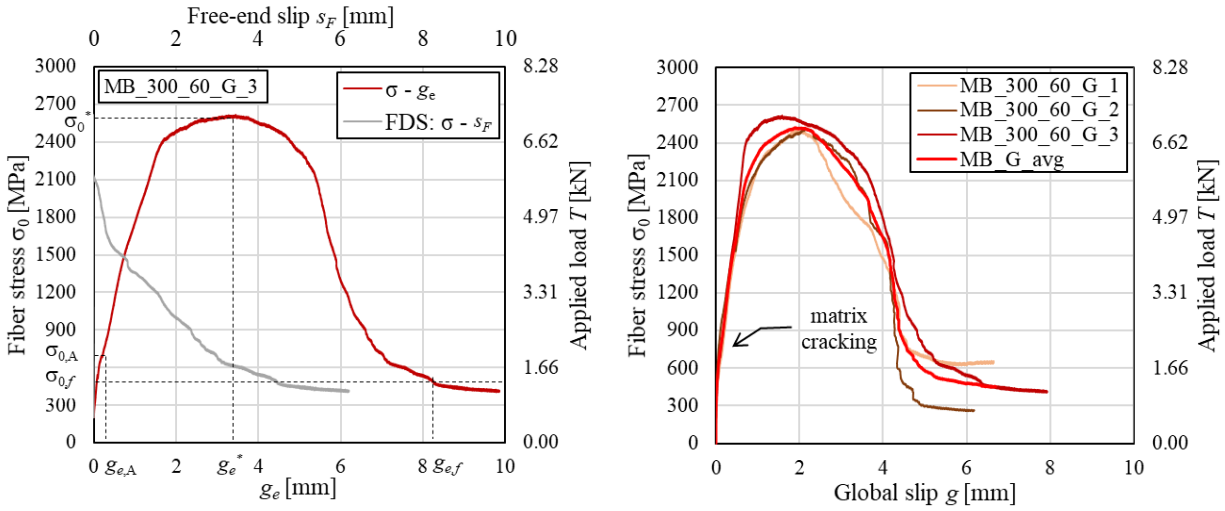

a. b.

Figure 5. Load responses of bond-gap MB tests: a) specimen MB_300_60_G_2 and b) specimens MB_300_60_G_1-3 [g was computed with Eq. (2)].

Based on these observations and taking into account the rotation of the concrete blocks (Figure 3b), the FDS global slip g for the MB tests with bond-gap layout was computed as:

$$\begin{cases} g = \dfrac{g_e}{2}\left[\dfrac{\cos(2\alpha)}{\cos\alpha}\right] & g_e \le g_{e,A} \\ g = \left(\dfrac{g_e}{2} - \dfrac{|\sigma_0 - \sigma_{0,A}|\, l_g}{2E_f}\right)\left[\dfrac{\cos(2\alpha)}{\cos\alpha}\right] & g_{e,A} < g_e \le g_e^* \\ g = \left(g_e - \dfrac{|\sigma_0 - \sigma_{0,A}|\, l_g}{E_f}\right)\left[\dfrac{\cos(2\alpha)}{\cos\alpha}\right] - g^* & g_e > g_e^* \end{cases} \quad (2)$$

where $\sigma_{0,A}$ and $g_{e,A}$ are the fiber stress at the first matrix crack and the corresponding average displacement measured by LVDTs G1 and G2 (see Figure 5a). The first equation in Eq. (2) describes the first branch of the $\sigma_0 - g$ curve, where the matrix is not cracked and the fibers contribution to the composite stress is neglected. The second and third equations in Eq. (2) are based on the assumption that the global slip is equal at the two loaded ends until the attainment of the peak fiber stress σ_0^*,

whereas it increases only at one loaded end after σ_0^*. These two latter equations also account for the elastic deformation of the PBO textile along the bond gap length l_g=60 mm (Figure 1c), which should not be included in the global slip g.

Assuming rigid rotation of the concrete blocks, the rotation angle α can be expressed as:

$$\alpha(g) = \arcsin\left(\frac{g}{h}\right) \tag{3}$$

where h (Figure 3b) is the vertical distance between the fiber exit point and the center of rotation of the block. It should be noted that Eq. (3) assumes the fiber exit point coincident with the block edge. The system of non-linear equations comprising Eqs. (2) and (3) provides, given the LVDT readings g_e, the global slip g and the angle α throughout the entire bond-gap MB test. The fiber stress σ_0 – global slip g curves of specimens MB_300_60_G_1-3 obtained with Eqs. (2) and (3) are reported in Figure 5b. Figure 5b shows that, at completion of the test, the fiber stress plateaued at a constant value $\sigma_{0,f}$ associated with friction at the matrix-fiber interface [30,37].

4.3 Direct shear test

The load response obtained by DS tests is shown in Figure 6a, whereas a photo of specimen DS_300_60_1 is shown in Figure 6b. In single-lap direct shear tests, the eccentricity between the force applied to the fiber and the support restraint entails for the presence of a bending moment that induces a Mode-I loading condition at the matrix-fiber interface. Since the presence of the external (i.e. not in contact with the support) matrix layer limits the effect of this Mode-I loading condition, a pure Mode-II loading condition can be postulated at the matrix-fiber interface. Therefore, the axial stress σ of DS tests was simply obtained as the ratio of the force applied by the machine and the cross-sectional area of the fibers A, whereas the global slip g was computed as the average of the displacement measured by LVDTs at the loaded end (Figure 1e).

Similarly to modified beam test, the curves showed an initial linear branch until micro-cracking occurred at the matrix-fiber interface and the response became non-linear. After the attainment of the

peak axial stress σ^*, a softening behavior was observed, i.e. the applied stress decreased with increasing the global slip g. At completion of the test, the applied stress plateaued at a constant value σ_f associated with friction at the matrix-fiber interface [30,37].

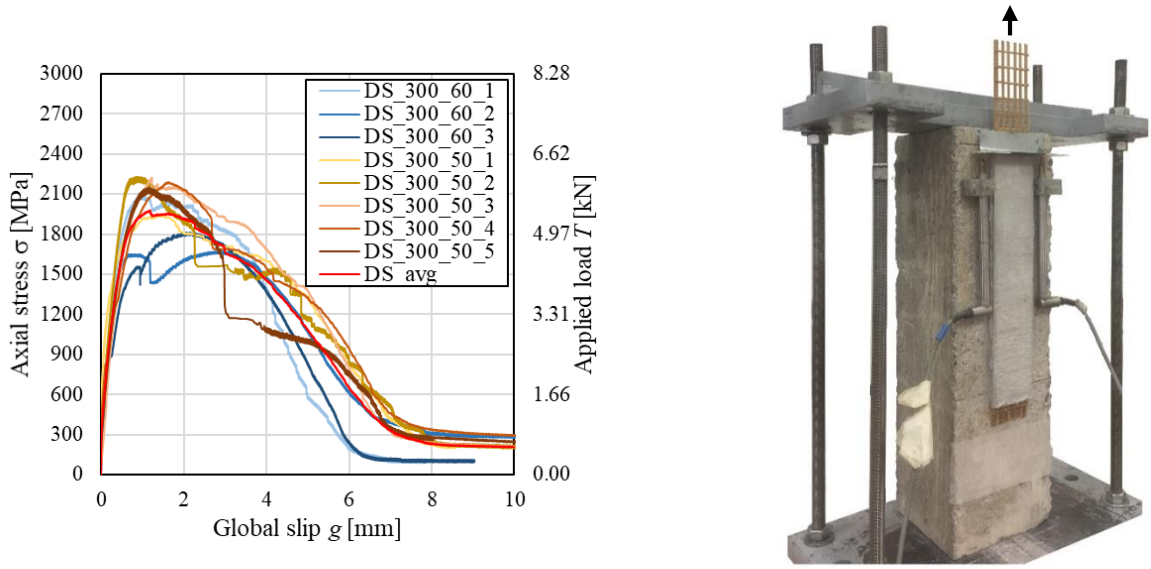

a. b.

Figure 6. a) Load responses of DS tests. b) Direct shear test setup.

5 Discussion

Key parameters obtained from MB and DS tests are reported in Table 1 and Table 2, respectively, along with average values of nominally equal specimens and corresponding coefficient of variation (CoV). Key parameters include the peak fiber stress σ_0^*(or axial stress σ^* for DS test), corresponding global slip g^*, residual friction fiber stress $\sigma_{0,f}$ (or axial stress σ_f for DS test), and the corresponding global slip g_f. According to [30], the residual stresses $\sigma_{0,f}$ and σ_f were computed as the average applied stress at the end of the test for which the derivative $d\sigma_0/dg$ or $d\sigma/dg$ were comprised within the range -200 and 0 MPa/mm. The value of g_f was defined as the first global slip value for which the inequalities $-200 \leq d\sigma_0/dg \leq 0$ MPa/mm or $-200 \leq d\sigma/dg \leq 0$ MPa/mm hold [31].

The envelopes of load responses of nominally equal MB and DS specimens are compared in Figure 7a. The results obtained showed that, although the same composite bonded length was considered for

MB and DS tests, the average peak fiber stress $\bar{\sigma}_0^*$ of bond-gap and bare-fiber MB tests ($\bar{\sigma}_0^*$=2543 MPa and $\bar{\sigma}_0^*$=2159 MPa, respectively) was 24.8% and 5.9% higher than that of DS tests ($\bar{\sigma}^*$=2038 MPa). This difference may be attributed to the presence of a fiber stress component, σ_I, normal to the matrix-fiber interface, induced by the specimen deflection in MB tests (Figure 3a).

The normal component σ_I is proportional to the cross-section curvature and tends to enhance the specimen bond capacity generating an additional frictional force at the matrix-fiber interface [46]. The normal component σ_I depends on the variation of the fiber axial direction along the bonded length. Due to the specimen deflection, the fiber pushes against the matrix internal layer (i.e. the matrix layer in contact with the concrete substrate), which deforms determining a variation of the fiber axial direction and, in turn, the presence of a normal stress component. Therefore, the stress component σ_I varies along the bonded length and its evaluation is cumbersome. Assuming rigid rotation of the concrete prisms comprising the MB specimen and neglecting the matrix deformability, σ_I can be assumed as concentrated at the strip loaded end in bare-fiber MB tests and at the bond gap (where matrix crack occurs) in bond-gap MB tests (Figure 3a). This simplification allows for studying the global effect of the normal force component on the FRCM-concrete bond behavior, as previously done for FRCM-masonry MB tests [31]. It should be noted that the presence of a stress component normal to the fiber longitudinal direction and concentrated at the fiber exit point, i.e. the matrix crack edge, was previously observed in fiber-reinforced concrete and its effect was named snubbing-friction effect [46,47].

σ_I can be assumed proportional to the angle of inclination of the fiber with respect to the matrix-fiber interface α [31,46,47], which coincides with the angle of rotation of the concrete prisms. Therefore, the snubbing-friction effect is particularly pronounced at the end of the test, when the specimen deflection is maximum. Accordingly, the average residual fiber stress $\bar{\sigma}_{0,f}$ of bond-gap and bare-

fiber MB tests ($\bar{\sigma}_{0,f}$ =463 MPa and $\bar{\sigma}_{0,f}$ =370 MPa, respectively) was 101.3% and 60.9% higher than the corresponding residual axial stress of DS tests ($\bar{\sigma}_{f}$ =230 MPa).

However, the presence of a normal stress component was also responsible for the rupture of some fiber filaments in MB tests, as revealed by visual inspection of the fibers at the loaded ends and at matrix cracks at the end of the test. This fiber damage, previously observed in carbon and PBO FRCM-masonry bare-fiber MB tests [31], appeared more pronounced in the case of bare-fiber layout than in the case of bond-gap layout. In bare-fiber specimens, the average peak fiber stress $\bar{\sigma}_{0}^{*}$ =2159 MPa and residual fiber stress $\bar{\sigma}_{0,f}$ =370 MPa were 15.1% and 20.1%, respectively, lower than those of bond-gap specimens ($\bar{\sigma}_{0}^{*}$ =2543 MPa and $\bar{\sigma}_{0,f}$ =463 MPa). This difference can be attributed to the presence of the matrix along the entire length of the strip in bond-gap specimens, which may have mitigated the fiber damage caused by the matrix-fiber friction at the fiber exit points.

Figure 7b shows the envelopes of fiber stress σ_0 – midspan deflection δ curves of bare-fiber and bond-gap MB tests, where δ is the average of the two vertical LVDTs V1 and V2 (Figure 1b and c). According to Figure 7b, bond-gap specimens provided higher maximum midspan deflections than bare-fiber MB tests. This confirms the influence of the normal stress component σ_I on the specimen capacity. Since bare-fiber and bond-gap specimens have the same geometry (except for the absence of matrix along the bond gap in the former specimens), the attainment of a higher midspan deflection in bond-gap specimens was attributed to the low damage to the fiber, which in turn allowed high values of σ_I and σ_0^*.

Finally, the result scatter observed in MB and DS tests was similar. The highest scatter was obtained for residual stress values (CoV=0.422 and CoV=0.406 for bond-gap and bare-fiber MB tests, respectively; CoV=0.350 for DS tests), whereas lower scatter was reported for peak stress values (CoV=0.025 and CoV=0.024 for bond-gap and bare-fiber MB tests, respectively; CoV=0.102 for DS tests). This result scatter can be considered small if compared with those reported in the literature for

FRCM composite bond tests [8,13,18]. However, it suggests the need of performing a large number of tests to obtain reliable measures of the bond properties.

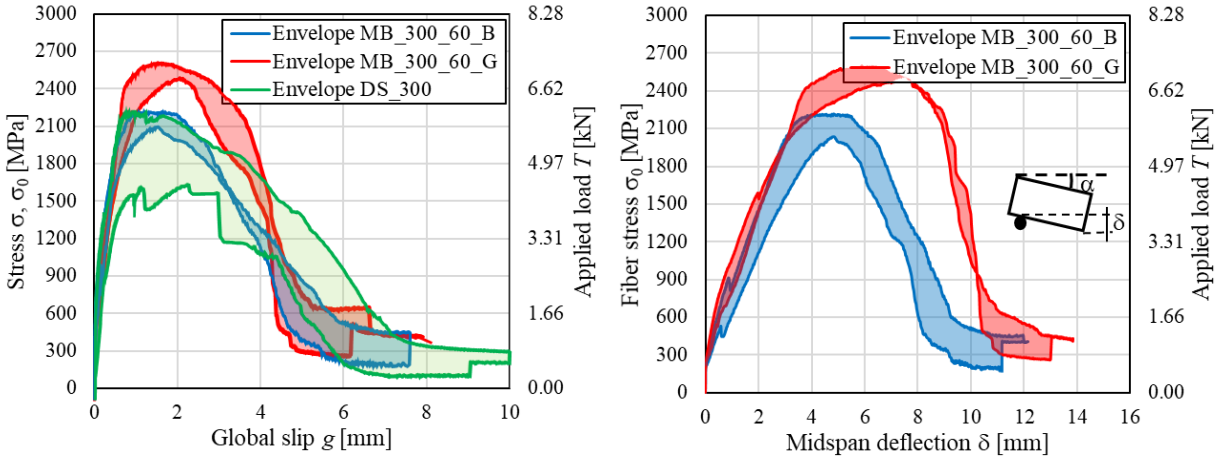

a. b.

Figure 7. Envelopes of a) σ_0 - and σ - g curves of MB and DS tests, respectively, and b) σ_0 - δ curves of MB tests.

6 Analytical study of the debonding process

Since the presence of a normal component at the matrix-fiber interface affects the composite bond behavior, the relationship between the fiber stress of MB tests (where the normal component is present) and axial stress of DS tests (where the normal component can be neglected), may be described by the function $\rho(g)$, which relates the fiber stress $\sigma_0(g)$ of MB tests ($\alpha \neq 0$) and the axial stress $\sigma(g)$ of DS tests ($\alpha=0$) for a given global slip g (see Figure 3a):

$$\rho(g) = \frac{\sigma_0(g)}{\sigma(g)} \tag{4}$$

It should be noted that Eq. (4) is based on the assumption that the global slip g is not affected by the test se-up, i.e. g is not influenced by the presence of σ_I. This assumption is supported by the similar average values of global slip at peak stress $\bar{g}^*$ obtained by the different test set-ups ($\bar{g}^*$=1.83 mm, 1.87 mm, and 1.53 mm for bond-gap and bare-fiber MB tests and for DS tests, respectively – see

Table 1 and Table 2). Li et al. (1990) employed Eq. (4) to describe the relationship between the maximum force obtained from fiber pull-out test with fiber inclined at an angle $\alpha \neq 0$ and that of the same fiber with $\alpha=0$. According to the experimental results of pull-out tests on nylon and polypropylene fibers embedded within a concrete matrix (25 mm bonded length), they proposed an exponential shape of $\rho(\alpha)$ [46]:

$$\rho(\alpha) = e^{(\alpha\mu)} \tag{5}$$

where μ is the snubbing friction coefficient [46]. Eqs. (5) and (4) are related by Eq. (3). Therefore, as a first attempt to correlate the bond behavior of DS and MB tests, in this paper the increase of bond capacity observed in MB tests with respect to DS tests is attributed to the snubbing-friction effect, which is assumed concentrated at the fiber exit point, and Eq. (5) [where α is obtained by Eq. (3)] is considered to describe the behavior of $\rho(g)$. The bending stiffness of the fiber was neglected according to the indication in [46]. The coefficient μ in Eq. (5) is a property of the specific FRCM composite and can be estimated experimentally with pull-out tests of fiber bundles embedded within matrix prisms varying the bonded length and angle of inclination of the pulling force [46]. It should be noted that more complex approaches were adopted to model the bond behavior of FRP and FRCM composites bonded to curved substrates [20,32,33]. However, in these cases the constant curvature of the substrate allowed for a simple solution of the problem, whereas the variation of the bending moment along the axis of the modified beam would require the use of cumbersome analytical or numerical methods.

Provided the function ρ, the composite bond behavior observed in MB tests can be described by computing σ from the bond differential equation obtained assuming a pure Mode-II loading condition (see Section 6.1) and then computing the fiber stress σ_0 accounting for the presence of the snubbing-friction effect substituting Eq. (4) into Eq. (5) and rearranging it:

$$\sigma_0 = \sigma e^{(\alpha\mu)} \tag{6}$$

6.1 Analytical solution of the bond differential equation accounting for the snubbing-friction effect

Under a pure Mode-II loading condition, the equilibrium of an infinitesimal segment of one fiber bundle of length *dx* embedded within the inorganic matrix (Table 3) provides the bond differential equation [48]:

$$\frac{d^2 s}{dx^2} - \frac{p}{EA_f}\tau(s) = 0 \tag{7}$$

where A_f, p, and E are the single fiber bundle cross-sectional area, perimeter, and elastic modulus, respectively. Provided the cohesive material law (CML), Eq. (7) can be solved to obtain the distribution of slip s, shear stress τ, and fiber strain ε along the bonded length L. The fiber axial stress at the loaded end σ and global slip g can then be obtained as $\sigma=E\varepsilon(L)$ and $g=s(L)$.

In this paper, a rigid-softening CML with a residual friction branch (Figure 8) was considered to describe the shear stress-slip relationship at the matrix-fiber interface [37].

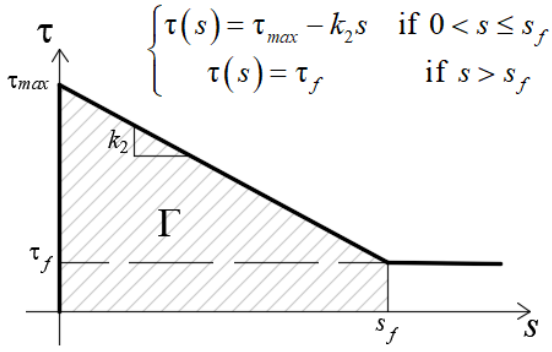

Figure 8. Rigid-softening CML.

For a bonded length L higher than the effective bond length l_{eff}, which is the interface length engaged in the bond stress-transfer mechanism, the CML law showed in Figure 8 provides four stages of the debonding process (Table 3):

- rigid-softening stage: a portion of interface of length L-l (see Table 3) is not stressed, whereas the remaining part of the interface of length l has a stress $\tau_{max}\geq\tau\geq\tau_f$;

- rigid-softening-debonding stage: the interface shear stress is equal to τ_f along the length a, is within $\tau_{max} \geq \tau \geq \tau_f$ along the length $l=l_{eff}$, and is zero for the remaining length L-a-l;
- softening-debonding stage: the interface shear stress is equal to τ_f along the length a, whereas the remaining length has a shear stress $\tau_{max} \geq \tau \geq \tau_f$.
- fully-debonded stage: the entire interface has a shear stress equal to τ_f.

Table 3. Fiber stress σ_0 and corresponding global slip g for each stage of the debonding process.

Stage	Fiber stress σ_0 – Global slip g equations	$\sigma(x)$ and $\tau(x)$ distributions
Problem formulation	$\frac{d^2 s}{dx^2} - \frac{p}{EA_f}\tau(s) = 0$	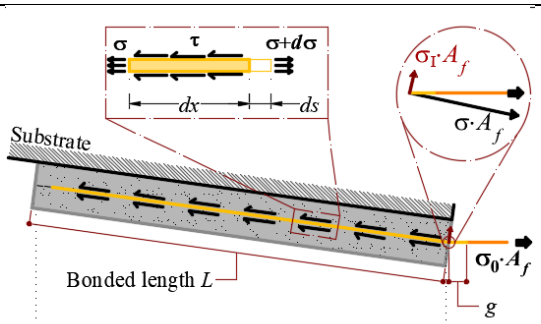
Rigid-Softening	$\begin{cases} \sigma_0 = \frac{p\tau_{max}}{\omega A_f}\sin(\omega l)e^{(\alpha\mu)} \\ g = \frac{\tau_{max}}{k_2}[1-\cos(\omega l)] \end{cases}$	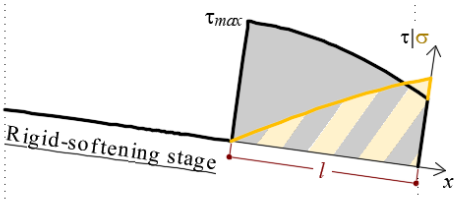
Rigid-Softening-Debonding	$\begin{cases} \sigma_0 = \left[\frac{p\tau_f a}{A_f} + \frac{p\tau_{max}}{\omega A_f}\sin(\omega l_{eff})\right]e^{(\alpha\mu)} \\ g = \frac{p\tau_f}{2EA_f}a^2 + \left[\frac{p\tau_{max}}{\omega EA_f}\sin(\omega l_{eff})\right]a + s_f \end{cases}$	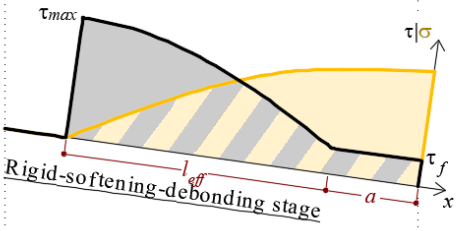
Softening-Debonding	$\begin{cases} \sigma_0 = \left\{\frac{p\tau_f a}{A_f} + \frac{p\tau_f}{\omega A_f}\tan[\omega(L-a)]\right\}e^{(\alpha\mu)} \\ g = \frac{p\tau_f}{2EA_f}a^2 + \frac{p\tau_f}{\omega EA_f}\tan[\omega(L-a)]a + s_f \end{cases}$	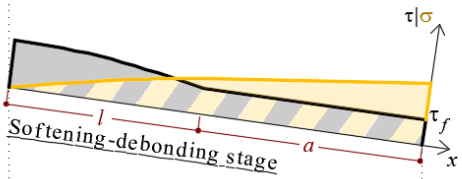
Fully-debonded	$\begin{cases} \sigma_0 = \frac{p\tau_f L}{A_f}e^{(\alpha\mu)} \\ g = \frac{p\tau_f}{2EA_f}L^2 + s_f \end{cases}$	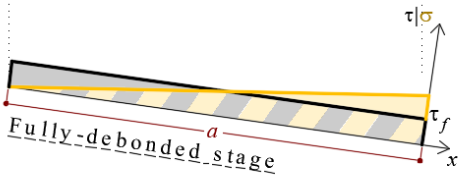

Note: $\omega^2 = \frac{pk_2}{EA_f}$, $l_{eff} = \frac{1}{\omega}\arccos\left(\frac{\tau_f}{\tau_{max}}\right)$.

438 The fiber stress at the loaded end σ_0 and corresponding global slip g obtained by substituting the
439 solution of Eq. (7) into Eq. (6) are reported in Table 3 for each stage. Further details about the solution
440 of Eq. (7) using the rigid-softening CML can be found in [37].
441
442 ***6.2 Calibration of the CML for DS tests***
443 As a first step, the CML was calibrated from the results of DS tests, where α=0. The rigid-softening
444 CML adopted is characterized by five parameters, namely τ_{max}, τ_f, k_2, s_f, and the area below the curve
445 up to s_f (Γ in Figure 8 [37]). When three of these parameters are known, the CML can be fully defined.
446 Different strategies can be adopted to estimate the CML parameters, comparing key points of the
447 analytical response with corresponding experimental values [37]. In this paper, the CML was
448 estimated by enforcing: (i) the residual axial stress σ_f at the end of the softening-debonding stage, (ii)
449 the peak axial stress σ^*, attained at the end of the rigid-softening-debonding stage, and (iii) the
450 effective bond length l_{eff}. The residual axial stress $\bar{\bar{\sigma}}_f$ and peak axial stress $\bar{\bar{\sigma}}^*$ of the average curves,
451 i.e. the load responses obtained by averaging the axial stress σ of nominally equal specimens for a
452 given g, were considered in the estimation of the CML. Values of $\bar{\bar{\sigma}}_f$ and $\bar{\bar{\sigma}}^*$ of the average curves
453 of DS tests (DS_avg) are reported in Table 2, whereas values of $\bar{\bar{\sigma}}_{0,f}$ and $\bar{\bar{\sigma}}_0^*$ of bare-fiber
454 (MB_B_avg) and bond-gap (MB_G_avg) in Table 1.
455 According to condition (i), the residual axial stress $\bar{\bar{\sigma}}_f$ of curve DS_avg (shown in Figure 6a) was
456 used to obtain the τ_f (see fully-debonded stage in Table 3):

457 $$\tau_f = \frac{A_f \bar{\bar{\sigma}}_f}{pL} \tag{8}$$

458 Provided τ_f, τ_{max} and k_2 were obtained substituting the peak axial stress $\bar{\bar{\sigma}}^*$ of DS_avg curve in the
459 system of non-linear equations comprising [condition (ii)] the equation providing the stress associated
460 with the end of the rigid-softening-debonding stage (see Table 3) and [condition (iii)] the equation
461 providing the effective bond length l_{eff} [37]:

462
$$\begin{cases} \bar{\bar{\sigma}}^{*} = \dfrac{p\tau_f a}{A_f} + \dfrac{p\tau_{max}}{\omega A_f}\sin\left(\omega l_{eff}\right) \quad \text{where} \quad \omega^2 = \dfrac{pk_2}{EA_f} \\ l_{eff} = \dfrac{1}{\omega}\arccos\left(\dfrac{\tau_f}{\tau_{max}}\right) \end{cases} \tag{9}$$

463 where l_{eff} was assumed equal to 260 mm according to data available in the literature for the same PBO
464 FRCM composite considered in this study [38].

465 The solution of Eqs. (8) and (9) provided τ_{max}=0.517 MPa, τ_f = 0.035 MPa, and k_2=0.32 MPa/mm,
466 which entails for s_f =1.52 mm. The analytical σ - g response obtained is compared with the envelope
467 of experimental load responses of DS tests in Figure 9. This comparison shows that the CML
468 calibration strategy adopted was effective, since good agreement between the experimental and
469 analytical load responses was obtained except for the descending branch. For this branch, the
470 analytical solution shows a snap-back whereas an increase of the global slip g for decreasing values
471 of σ was observed experimentally. This difference is well-known for externally bonded composites
472 and was ascribed to the test control that did not allow for capturing the snap-back phenomenon [49].
473 Further details regarding the difference between the experimental and analytical descending branches
474 can be found in [37].

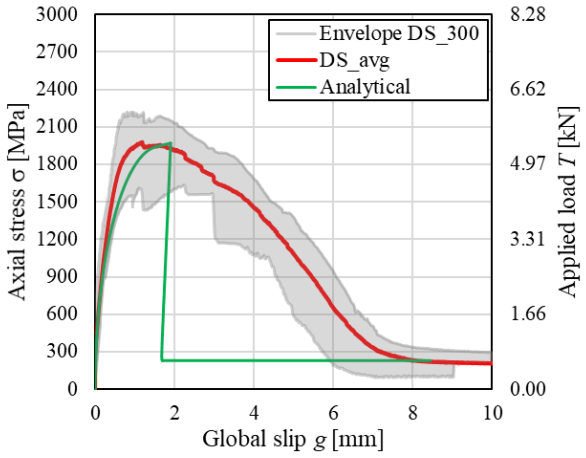

475

476 Figure 9. Comparison between analytical and experimental σ - g responses of DS tests.

477

6.3 Analytical model of MB tests

The bond behavior of MB tests with bond-gap layout was modeled using Eq. (6) with α measured in degrees [°] and defined by Eq. (3). The results of MB tests with bare-fiber layout were not modeled due to the presence of significant fiber damage, as discussed in Section 4.1. In Eq. (6), the axial stress σ was obtained from the CML calibrated using the DS tests in Section 6.2, the angle α and the global slip g were obtained from the displacement g_e (recorded by LVDTs G1 and G2) solving Eqs. (2) and (3). The snubbing friction coefficient μ was finally calibrated through a best-fitting analysis. Namely, μ was obtained by best fitting the experimental ratio ρ with the equation obtained substituting Eq. (3) into Eq. (5):

$$\rho(g) = \frac{\sigma_0(g)}{\sigma(g)} = e^{\left(\mu \arcsin\frac{g}{h}\right)} \tag{10}$$

where $\sigma_0(g)$ and $\sigma(g)$ are the fiber stress of bond-gap MB and axial stress of DS tests, respectively, for a given value of g (and, in turn, of α). The average curve $\sigma_0(g)$ of MB (MB_G_avg) and $\sigma(g)$ of DS (DS_avg) tests, which are reported in Figure 5b and Figure 6a, respectively, were considered in Eq. (10). The experimental ratio ρ obtained from the average experimental curves for $0<g\leq\hat{g}^*$ is reported in Figure 10a, where $\hat{g}^*$=1.89 mm is the global slip associated with the peak fiber stress of the MB_G_avg curve (Table 1). The response softening branch ($g>\hat{g}^*$) was not considered to evaluate ρ because the fiber was increasingly damaged during this phase in MB tests.

Figure 10a shows that, after an initial scattered stage (g<0.2 mm approximatively), the experimental ρ increases at an approximately constant rate until $\hat{g}^*$ is attained. The irregularity in the initial trend of ρ can be attributed to the variability of the load responses at the beginning of the test, which are mainly governed by the portion of bonded length close to the loaded end. Small misalignment of the textile with respect to the applied force direction in DS tests, adjustments of the modified beams, and randomly distributed properties of the matrix-fiber interface may induce scatter of the initial branch

of the load responses. With increasing the global slip, the area of matrix-fiber interface engaged in the stress-transfer increases and these differences become less significant.

The snubbing friction coefficient μ was obtained by best fitting the experimental ρ curve using Eq. (10) considering all data in Figure 10a, which provided μ=0.40 (R^2=0.82), and considering only points associated with the increasing rate of ρ, which provided μ=0.41 (R^2=0.91). The curve described by Eq. (10) with μ=0.40 is shown in Figure 10a. Since ρ obtained by Eq. (10) showed an approximately linear behavior, a further best fitting of the experimental ρ curve was performed considering a linear equation:

$$\rho(g) = 1 + \mu \arcsin\left(\frac{g}{h}\right) \tag{11}$$

Eq. (11) provided μ=0.45 (R^2=0.82) considering all data in Figure 10a and μ=0.46 (R^2=0.94) considering only points associated with the increasing rate of ρ. The ρ curve described by Eq. (11) with μ=0.45 is shown in Figure 10a.

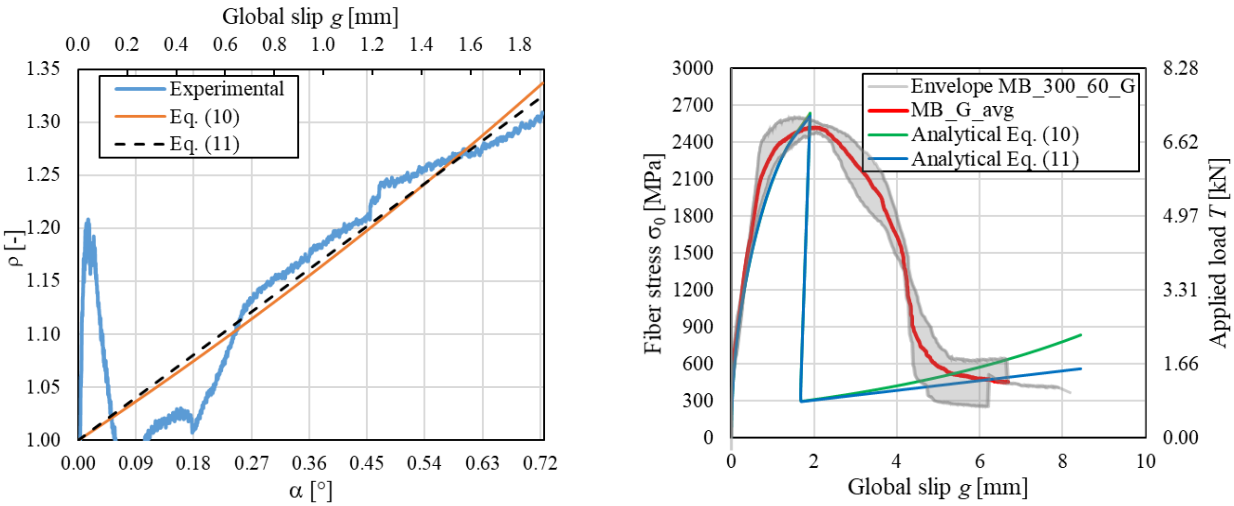

Figure 10. a) Experimental and fitted ρ curves. b) Comparison between analytical and experimental σ_0 - g responses of MB tests.

The analytical $\sigma_0 - g$ curve obtained by Eq. (6), where σ was computed solving the bond differential equation as explained in Sections 6.1 and 6.2 and assuming an exponential behavior of ρ [Eq. (10)] with μ =0.40, is compared with the MB_G_avg curve and the corresponding envelope in Figure 10b. This figure shows also the $\sigma_0 - g$ curve obtained by Eq. (6) assuming a linear behavior of ρ [Eq. (11)] with μ =0.45 (note that in this case the solution of the differential equation is the same reported in Table 3 substituting the term $e^{\mu\alpha}$ with $1+\mu\alpha$). The analytical curves show good agreement with the average load response during the ascending branch. The peak stresses attained by the analytical curves [σ_0^*=2638 MPa for Eq. (10) and σ_0^*=2614 MPa for Eq. (11)] are only slightly higher than the peak stress attained by the average curve MB_G_avg (σ_0^*=2522 MPa). As in the case of the DS tests, the $\sigma_0 - g$ experimental and analytical descending branches have a different behavior due to the presence of snap-back in the analytical solution (see Section 6.2). The final branches of the analytical curves, which are associated with the fully-debonded stage in Table 3, show increasing values of the fiber stress associated with friction. This behavior, which is caused by the increase of the angle α with increasing *g*, can be observed for specimen MB_300_60_G_1 (Figure 5), whereas it was not present in the remaining specimens due to the occurrence of fiber damage. The increase of the fiber stress during the fully-debonded stage was observed in MB tests comprising masonry blocks and PBO FRCM strips [31].

7 Conclusions

In this paper, a direct shear and a modified beam test set-up were employed to study the bond behavior of a PBO FRCM composite bonded to a concrete substrate. Two different strip layouts, differing for the presence or not of the embedding matrix at the specimen midspan, were investigated in the modified beam tests. Based on the load responses observed for the different set-ups, an analytical approach able to account for the presence of stresses normal to the matrix-fiber interface was proposed. The results obtained allowed for drawing the following main conclusions:

- The load responses of DS and MB tests were similar. However, the presence of a stress component σ_I orthogonal to the matrix-fiber interface determined an average increase in the MB specimens bond capacity with respect to that of DS test of approximately 24.8% and 5.9% for bond-gap and bare-fibers specimens, respectively.
- The presence of σ_I induced damage of fiber filaments in the textile. This damage appeared more pronounced in the case of bare-fiber layout than in the case of bond-gap layout.
- The rigid-softening CML, calibrated on key points of the DS test average curve, allowed for obtaining an analytical response in good agreement with experimental results.
- The analytical approach proposed was able to accurately reproduce the load response of bond-gap modified beam tests starting from the CML calibrated on the results of direct shear tests.
- The relationship between the fiber stress of MB tests and axial stress of DS tests can be described by an exponential or a linear function depending on the rotation angle and on the snubbing friction coefficient.

Acknowledgements

The experimental tests described were carried out at the Structural Material Lab of the Politecnico di Milano. Ruregold Srl is gratefully acknowledged for providing the FRCM composite.

Data availability statement

The raw/processed data required to reproduce these findings cannot be shared at this time as the data also forms part of an ongoing study.

References

[1] Donnini J, Spagnuolo S, Corinaldesi V. A comparison between the use of FRP, FRCM and HPM for concrete confinement. Compos Part B 2019;160:586–94. https://doi.org/10.1016/j.compositesb.2018.12.111.

[2] Faleschini F, Zanini MA, Hofer L, Toska K, De Domenico D, Pellegrino C. Confinement of reinforced concrete columns with glass fiber reinforced cementitious matrix jackets. Eng Struct 2020;218:110847. https://doi.org/10.1016/j.engstruct.2020.110847.
[3] D'Ambrisi A, Focacci F. Flexural Strengthening of RC Beams with Cement-Based Composites. J Compos Constr 2011;15:707–20. https://doi.org/10.1061/(ASCE)CC.1943-5614.0000218.
[4] Babaeidarabad S, Loreto G, Nanni A. Flexural Strengthening of RC Beams with an Externally Bonded Fabric-Reinforced Cementitious Matrix. J Compos Constr 2014;18:04014009. https://doi.org/10.1061/(ASCE)CC.1943-5614.0000473.
[5] Younis A, Ebead U, Shrestha KC. Different FRCM systems for shear-strengthening of reinforced concrete beams. Constr Build Mater 2017;153:514–26. https://doi.org/10.1016/j.conbuildmat.2017.07.132.
[6] Ombres L, Verre S. Shear performance of FRCM strengthened RC beams. ACI SP-324, vol. 2017- March, Gianmarco de Felice, Lesley H. Sneed, Antonio Nanni; 2018.
[7] Prota A, Marcari G, Fabbrocino G, Manfredi G, Aldea C. Experimental In-Plane Behavior of Tuff Masonry Strengthened with Cementitious Matrix–Grid Composites. J Compos Constr 2006;10:223–33. https://doi.org/10.1061/(ASCE)1090-0268(2006)10:3(223).
[8] D'Antino T, Carozzi FG, Colombi P, Poggi C. Out-of-plane maximum resisting bending moment of masonry walls strengthened with FRCM composites. Compos Struct 2018;202:881–96. https://doi.org/10.1016/j.compstruct.2018.04.054.
[9] Valluzzi MR, da Porto F, Garbin E, Panizza M. Out-of-plane behaviour of infill masonry panels strengthened with composite materials. Mater Struct 2014;47:2131–45. https://doi.org/10.1617/s11527-014-0384-6.
[10] Alecci V, Focacci F, Rovero L, Stipo G, De Stefano M. Intrados strengthening of brick masonry arches with different FRCM composites: Experimental and analytical investigations. Composite Structures 2017;176:898–909. https://doi.org/10.1016/j.compstruct.2017.06.023.
[11] Wang X, Ghiassi B, Oliveira DV, Lam CC. Modelling the nonlinear behaviour of masonry walls strengthened with textile reinforced mortars. Eng Struct 2017;134:11–24. https://doi.org/10.1016/j.engstruct.2016.12.029.
[12] Al-Salloum YA, Almusallam TH, Elsanadedy HM, Iqbal RA. Effect of elevated temperature environments on the residual axial capacity of RC columns strengthened with different techniques. Constr Build Mater 2016;115:345–61. https://doi.org/10.1016/j.conbuildmat.2016.04.041.
[13] de Felice G, D'Antino T, De Santis S, Meriggi P, Roscini F. Lessons Learned on the Tensile and Bond Behavior of Fabric Reinforced Cementitious Matrix (FRCM) Composites. Front Built Environ 2020;6. https://doi.org/10.3389/fbuil.2020.00005.
[14] Banholzer B. Bond Behaviour of a Multi-Filament Yarn Embedded in a Cementitious Matrix. RETH Aachen University, 2004.
[15] Carozzi FG, Poggi C. Mechanical properties and debonding strength of Fabric Reinforced Cementitious Matrix (FRCM) systems for masonry strengthening. Comp Part B 2015;70:215–30. https://doi.org/10.1016/j.compositesb.2014.10.056.
[16] Santandrea M, Focacci F, Mazzotti C, Ubertini F, Carloni C. Determination of the interfacial cohesive material law for SRG composites bonded to a masonry substrate. Eng Fail Analys 2020;111:104322. https://doi.org/10.1016/j.engfailanal.2019.104322.
[17] National Research Council. Guide for the design and construction of externally bonded fibre reinforced inorganic matrix systems for strengthening existing structures. CNR-DT 215/2018. Rome, Italy: CNR; 2018.
[18] Koutas LN, Tetta Z, Bournas DA, Triantafillou TC. Strengthening of Concrete Structures with Textile Reinforced Mortars: State-of-the-Art Review. J Compos Constr 2019;23:03118001. https://doi.org/10.1061/(ASCE)CC.1943-5614.0000882.

[19] Askouni PD, Papanicolaou CG. Experimental investigation of bond between glass textile reinforced mortar overlays and masonry: the effect of bond length. Mater Struct 2017;50:164. https://doi.org/10.1617/s11527-017-1033-7.
[20] De Lorenzis L, Zavarise G. Interfacial stress analysis and prediction of debonding for a thin plate bonded to a curved substrate. International Journal of Non-Linear Mechanics 2009;44:358–70. https://doi.org/10.1016/j.ijnonlinmec.2009.01.002.
[21] Achintha M, Burgoyne CJ. Fracture mechanics of plate debonding: Validation against experiment. Constr Build Mater 2011;25:2961–71. https://doi.org/10.1016/j.conbuildmat.2010.11.103.
[22] Finckh W, Zilch K. Influence of the Curvature on the Bond Force Transfer of EBR. SP 2011;275:1–20. https://doi.org/10.14359/51682432.
[23] Federation Internationale du Beton. fib Bulletin 90. Externally applied FRP reinforcement for concrete structures. fib. The International Federation for Structural Concrete; 2019. https://doi.org/10.35789/fib.BULL.0090.
[24] Alecci V, Focacci F, Rovero L, Stipo G, De Stefano M. Extrados strengthening of brick masonry arches with PBO–FRCM composites: Experimental and analytical investigations. Compos Struct 2016;149:184–96. https://doi.org/10.1016/j.compstruct.2016.04.030.
[25] Pantò B, Cannizzaro F, Caddemi S, Caliò I, Chácara C, Lourenço PB. Nonlinear Modelling of Curved Masonry Structures after Seismic Retrofit through FRP Reinforcing. Buildings 2017;7:79. https://doi.org/10.3390/buildings7030079.
[26] Basilio I, Fedele R, Lourenço PB, Milani G. Assessment of curved FRP-reinforced masonry prisms: Experiments and modeling. Construction and Building Materials 2014;51:492–505. https://doi.org/10.1016/j.conbuildmat.2013.11.011.
[27] De Santis S. Bond behaviour of Steel Reinforced Grout for the extrados strengthening of masonry vaults. Construction and Building Materials 2017;150:367–82. https://doi.org/10.1016/j.conbuildmat.2017.06.010.
[28] Rotunno T, Fagone M, Bertolesi E, Grande E, Milani G. Curved masonry pillars reinforced with anchored CFRP sheets: An experimental analysis. Composites Part B: Engineering 2019;174:107008. https://doi.org/10.1016/j.compositesb.2019.107008.
[29] Malena M, de Felice G. Debonding of composites on a curved masonry substrate: Experimental results and analytical formulation. Compos Struct 2014;112:194–206. https://doi.org/10.1016/j.compstruct.2014.02.004.
[30] Calabrese AS, Colombi P, D'Antino T. A Bending Test Set-Up for the Investigation of the Bond Properties of FRCM Strengthenings Applied to Masonry Substrates. Key Eng Mater 2019. https://doi.org/10.4028/www.scientific.net/KEM.817.149.
[31] Calabrese AS, D'Antino T, Colombi P, Poggi C. Study of the influence of interface normal stresses on the bond behavior of FRCM composites using direct shear and modified beam tests. Constr Build Mater 2020;262:120029. https://doi.org/10.1016/j.conbuildmat.2020.120029.
[32] Malena M. Closed-form solution to the debonding of mortar based composites on curved substrates. Composites Part B: Engineering 2018;139:249–58. https://doi.org/10.1016/j.compositesb.2017.11.044.
[33] Biscaia HC, Chastre C, Silva MAG. Analytical model with uncoupled adhesion laws for the bond failure prediction of curved FRP-concrete joints subjected to temperature. Theoretical and Applied Fracture Mechanics 2017;89:63–78. https://doi.org/10.1016/j.tafmec.2017.01.008.
[34] Kafkalidis MS, Thouless MD. The effects of geometry and material properties on the fracture of single lap-shear joints. International Journal of Solids and Structures 2002;39:4367–83. https://doi.org/10.1016/S0020-7683(02)00344-X.
[35] Li S, Thouless MD, Waas AM, Schroeder JA, Zavattieri PD. Mixed-mode cohesive-zone models for fracture of an adhesively bonded polymer–matrix composite. Engineering Fracture Mechanics 2006;73:64–78. https://doi.org/10.1016/j.engfracmech.2005.07.004.

[36] Carloni C, D'Antino T, Sneed LH, Pellegrino C. Three-Dimensional Numerical Modeling of Single-Lap Direct Shear Tests of FRCM-Concrete Joints Using a Cohesive Damaged Contact Approach. J Compos Constr 2018;22:04017048. https://doi.org/10.1061/(ASCE)CC.1943-5614.0000827.
[37] Calabrese AS, Colombi P, D'Antino T. Analytical solution of the bond behavior of FRCM composites using a rigid-softening cohesive material law. Comp Part B 2019;174:107051. https://doi.org/10.1016/j.compositesb.2019.107051.
[38] D'Antino T, Carloni C, Sneed LH, Pellegrino C. Matrix–fiber bond behavior in PBO FRCM composites: A fracture mechanics approach. Eng Fract Mech 2014;117:94–111. https://doi.org/10.1016/j.engfracmech.2014.01.011.
[39] Calabrese AS, D'Antino T, Colombi P, Poggi C, Carloni C. Influence of the test set-up on the bond behavior of FRCM composites. ACI SP In publication.
[40] CSLLPP - Servizio Tecnico Centrale. Linee guida per la identificazione, la qualificazione ed il controllo di accettazione di compositi fibrorinforzati a matrice inorganica (FRCM) da utilizzarsi per il consolidamento strutturale di costruzioni esistenti. Rome, Italy: 2019.
[41] ASTM International. Standard Test Method for Evaluation of Performance for FRP Composite Bonded to Concrete Substrate using Beam Test. ASTM D7958/D7958M - 17. ASTM International; n.d. https://doi.org/10.1520/D7958_D7958M-17.
[42] Donnini J, Corinaldesi V. Mechanical characterization of different FRCM systems for structural reinforcement. Constr Build Mater 2017;145:565–75. https://doi.org/10.1016/j.conbuildmat.2017.04.051.
[43] Ombres L, Mancuso N, Mazzuca S, Verre S. Bond between Carbon Fabric-Reinforced Cementitious Matrix and Masonry Substrate. J Mater Civil Eng 2019;31:04018356. https://doi.org/10.1061/(ASCE)MT.1943-5533.0002561.
[44] D'Antino T, Focacci F, Carloni C, Sneed LH. Relationship between the effective strain of FRCM-strengthened RC beams and the debonding strain of direct shear tests. Engineering Structures 2020. https://doi.org/10.1016/j.engstruct.2020.110631.
[45] Calabrese AS, D'Antino T, Colombi P, Poggi C. Study of the bond behavior of FRCM-masonry joints using a modified beam test. Proceedings of the twenty-fourth Italian Association of Theoretical and Applied Mechanics Convention (AIMETA 2019), Rome, Italy: The Italian Association of Theoretical and Applied Mechanics; 2019.
[46] Li VC, Wang Y, Backer S. Effect of inclining angle, bundling and surface treatment on synthetic fibre pull-out from a cement matrix. Composites 1990;21:132–40. https://doi.org/10.1016/0010-4361(90)90005-H.
[47] Fu S-Y, Lauke B. The fibre pull-out energy of misaligned short fibre composites. J Mater Sci 1997;32:1985–93. https://doi.org/10.1023/A:1018593931951.
[48] Täljsten B. Strengthening of Beams by Plate Bonding. Journal of Materials in Civil Engineering 1997;9:206–12. https://doi.org/10.1061/(ASCE)0899-1561(1997)9:4(206).
[49] Carrara P, Ferretti D, Freddi F, Rosati G. Shear tests of carbon fiber plates bonded to concrete with control of snap-back. Eng Fract Mech 2011;78:2663–78. https://doi.org/10.1016/j.engfracmech.2011.07.003.

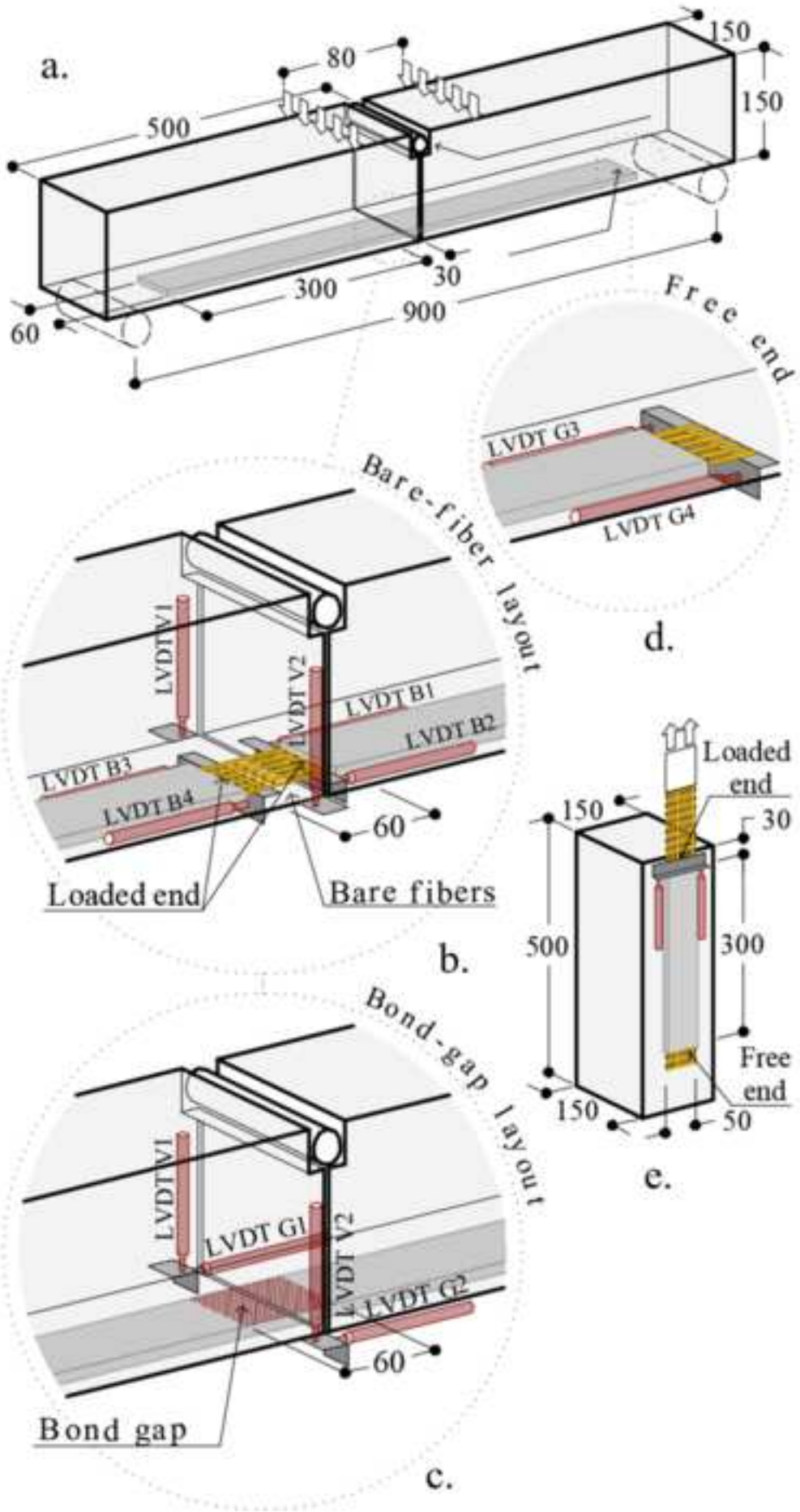

Figure_2a

Click here to access/download;Figure;Figure_2a.tiff

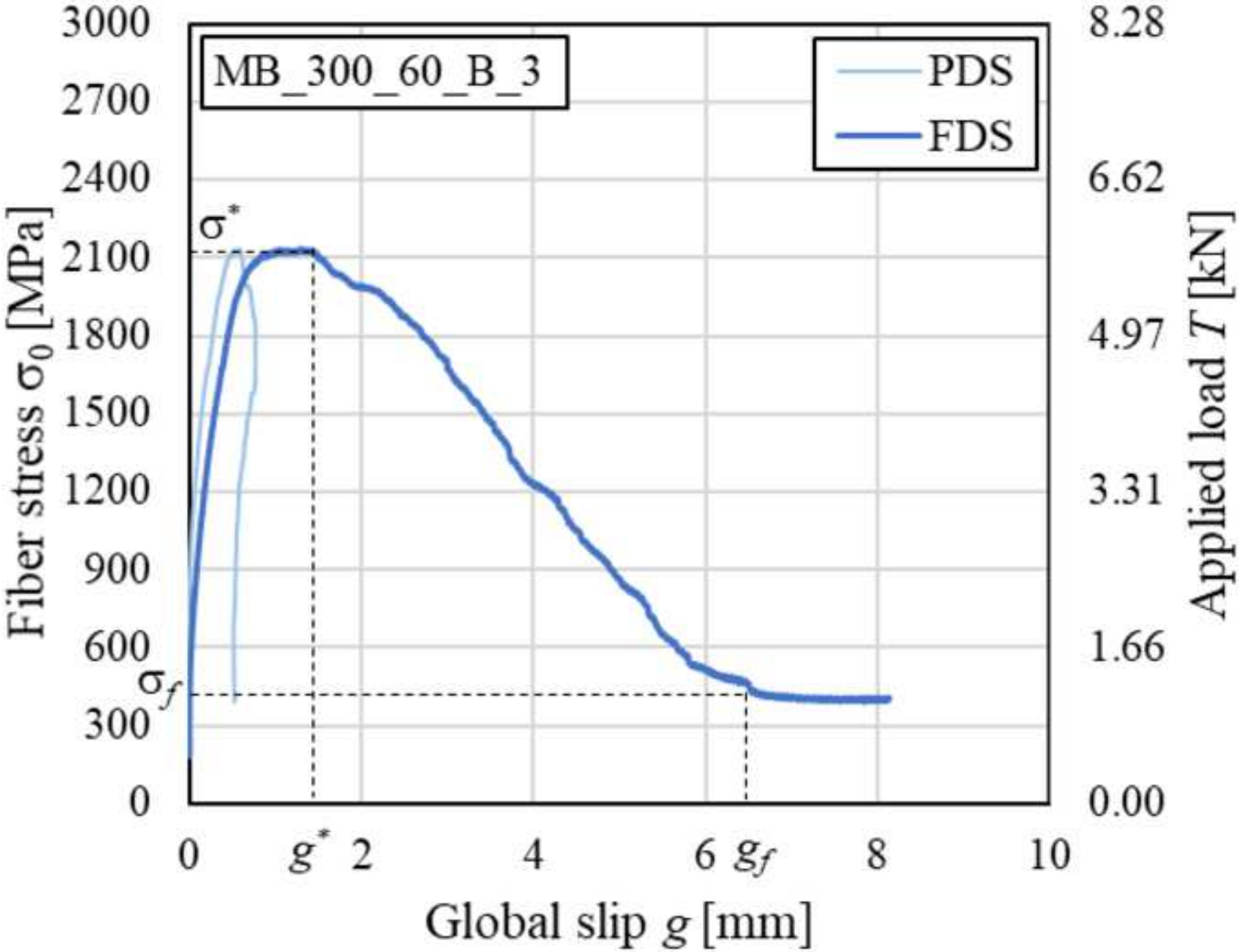

Figure_2b

Click here to access/download;Figure;Figure_2b.tiff

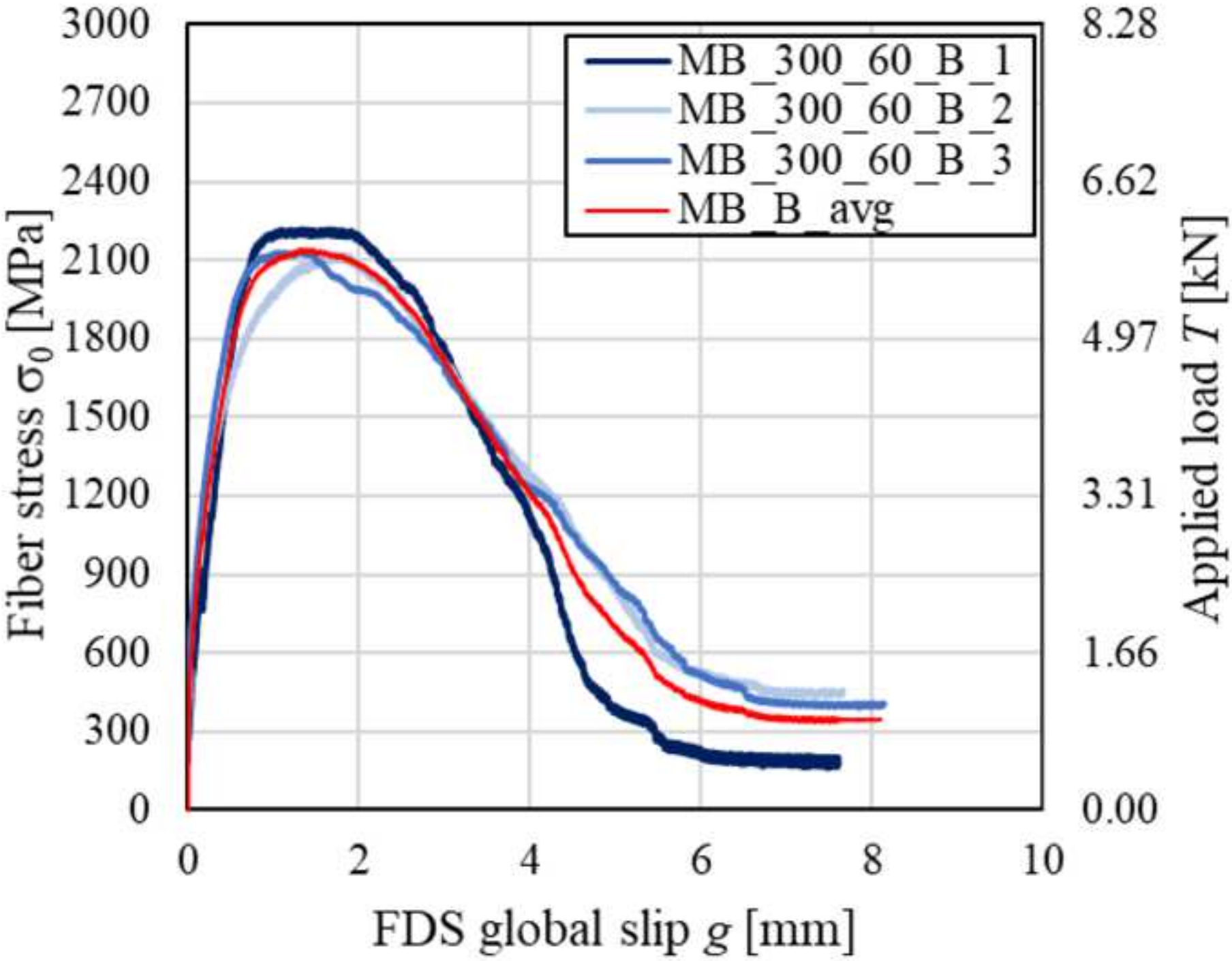

Figure_3a

Click here to access/download;Figure;Figure_3a.tiff

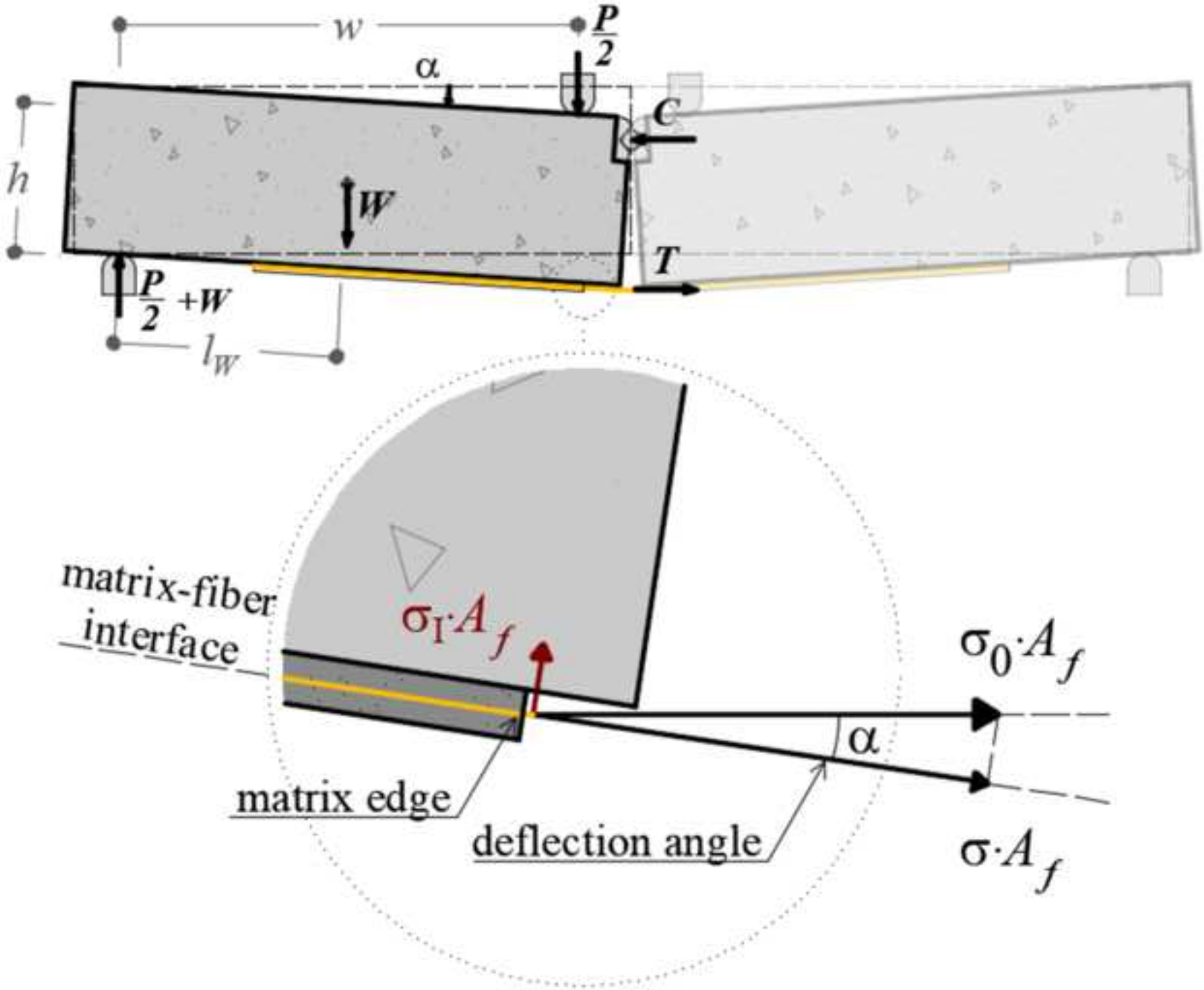

Figure_3b

Click here to access/download;Figure;Figure_3b.tiff

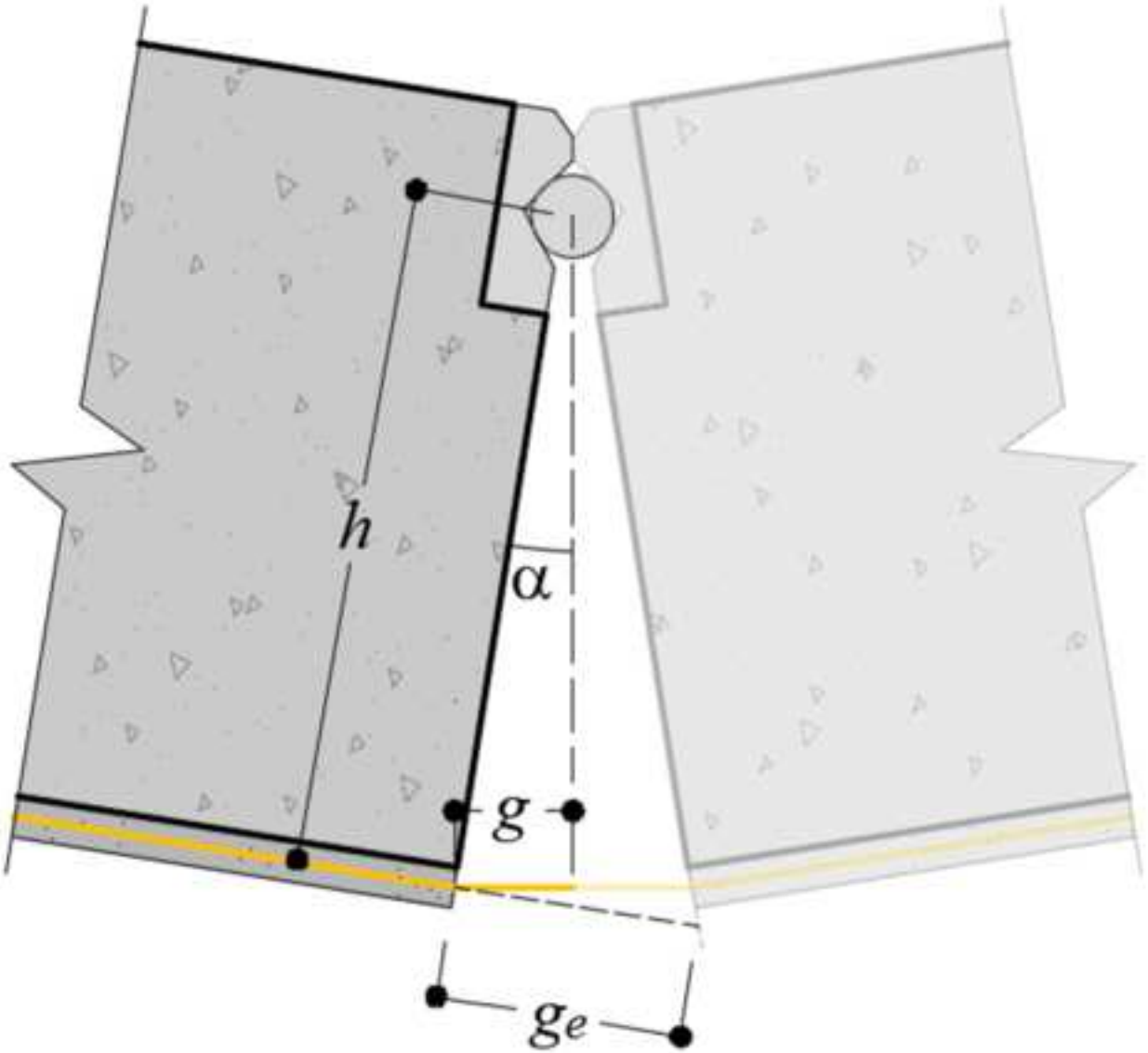

Figure_4a-c

Click here to access/download;Figure;Figure_4a-c.tiff

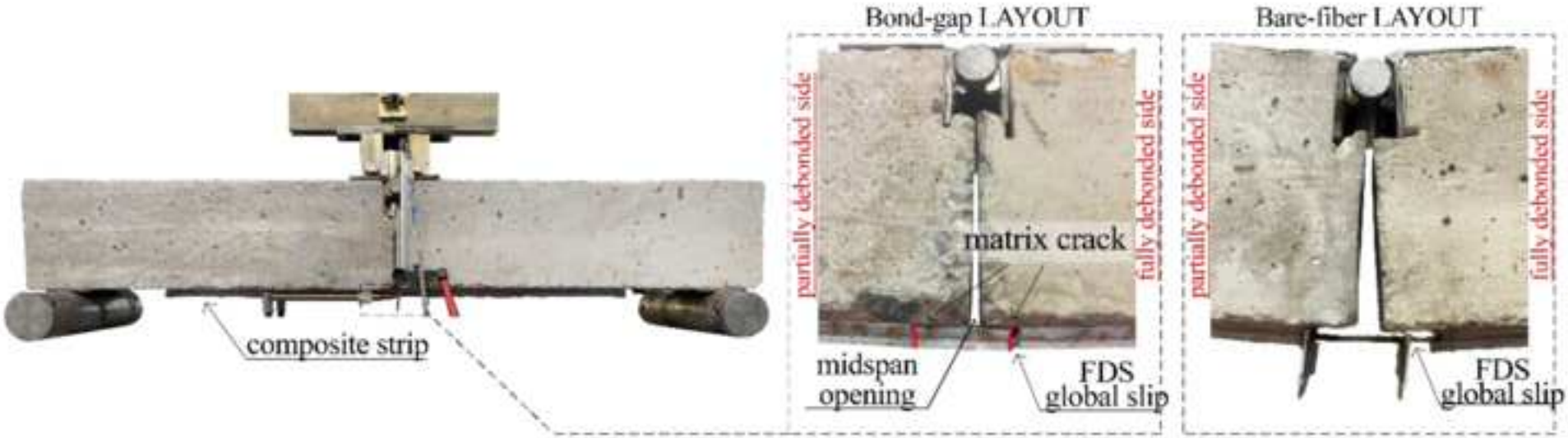

Figure_5a

Click here to access/download;Figure;Figure_5a.tiff

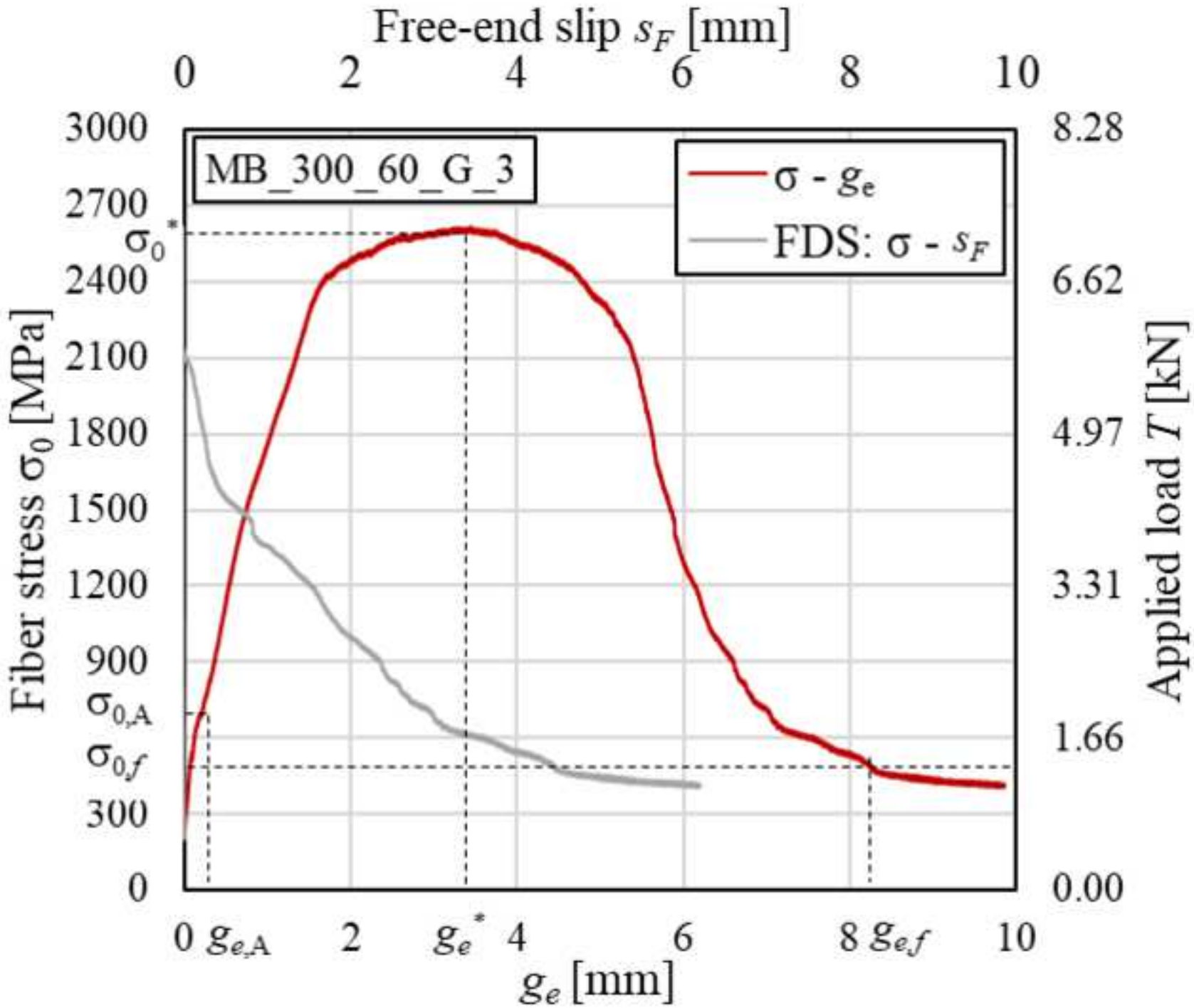

Figure_5b

Click here to access/download;Figure;Figure_5b.tiff

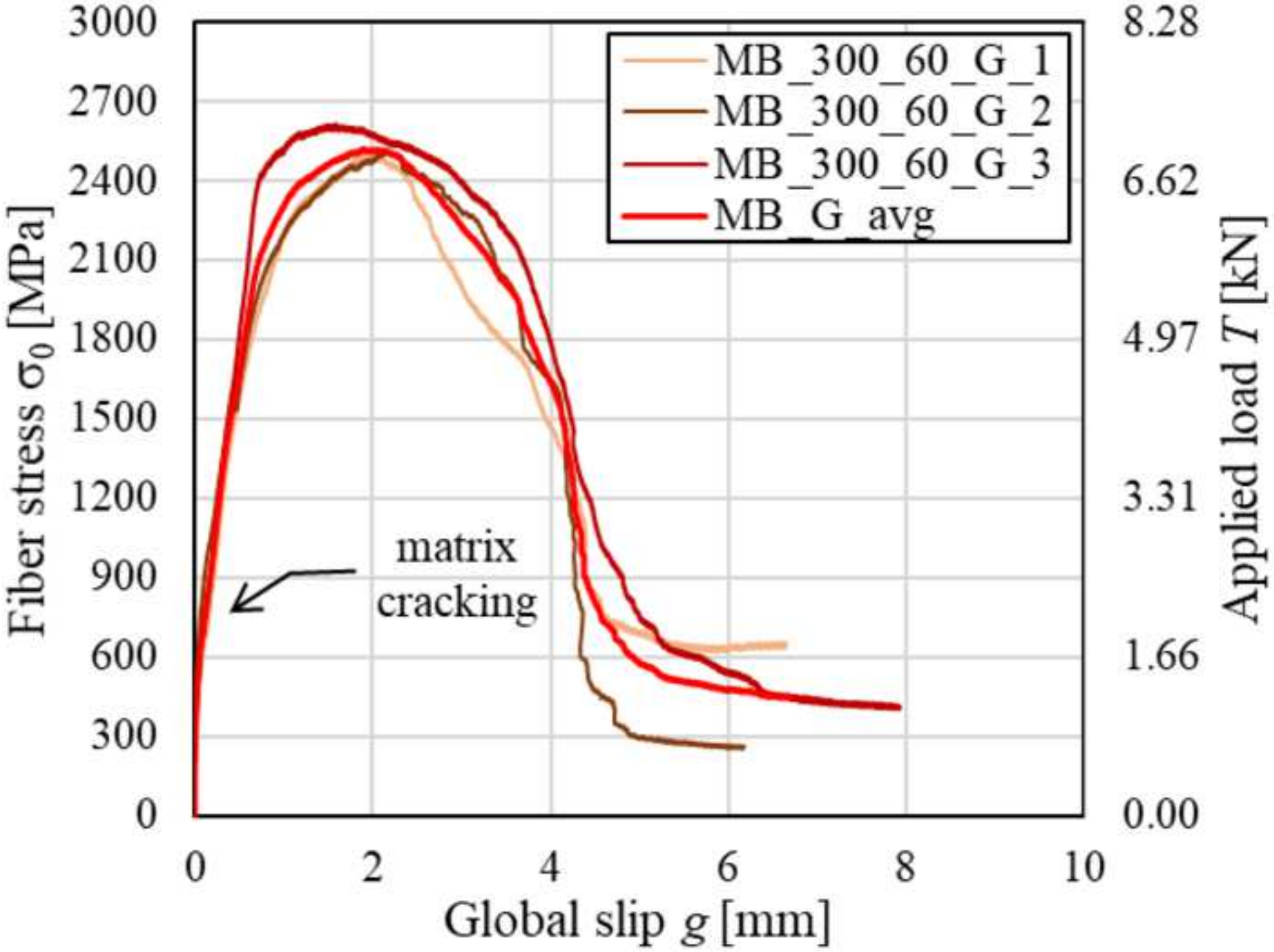

Figure_6a

Click here to access/download;Figure;Figure_6a.tiff

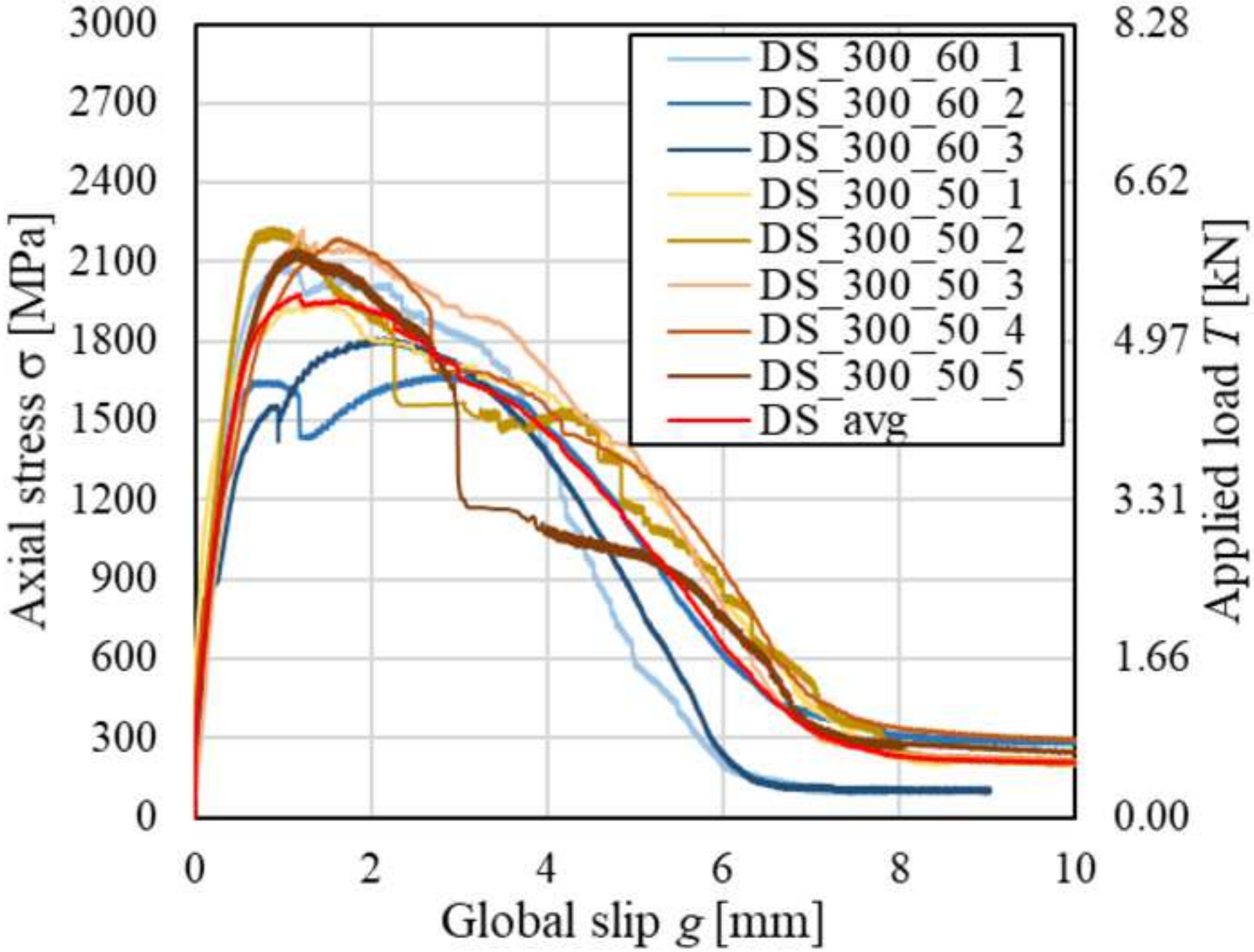

Figure_6b

Click here to access/download;Figure;Figure_6b.tiff

Figure_7a

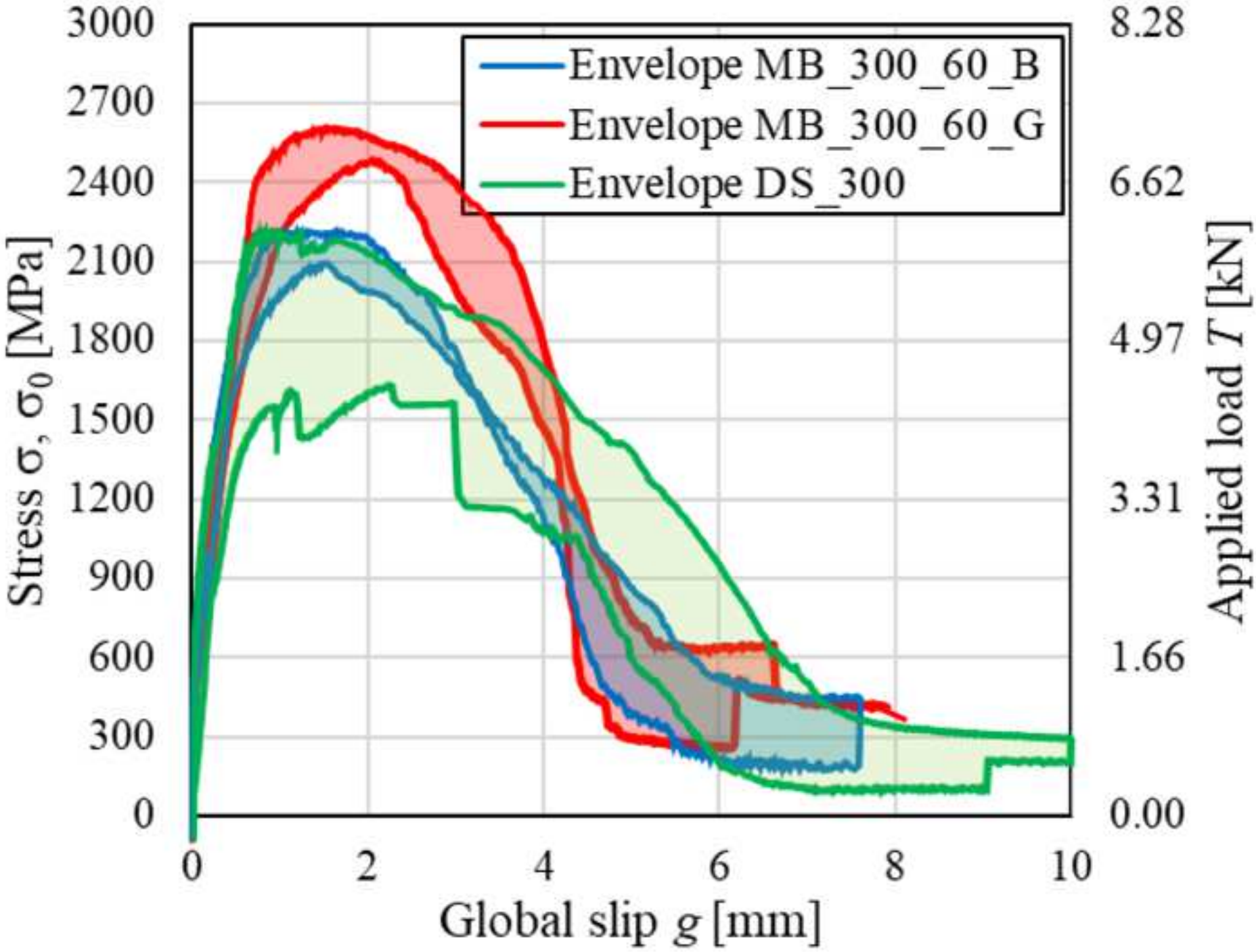

Figure_7b

Click here to access/download;Figure;Figure_7b.tiff

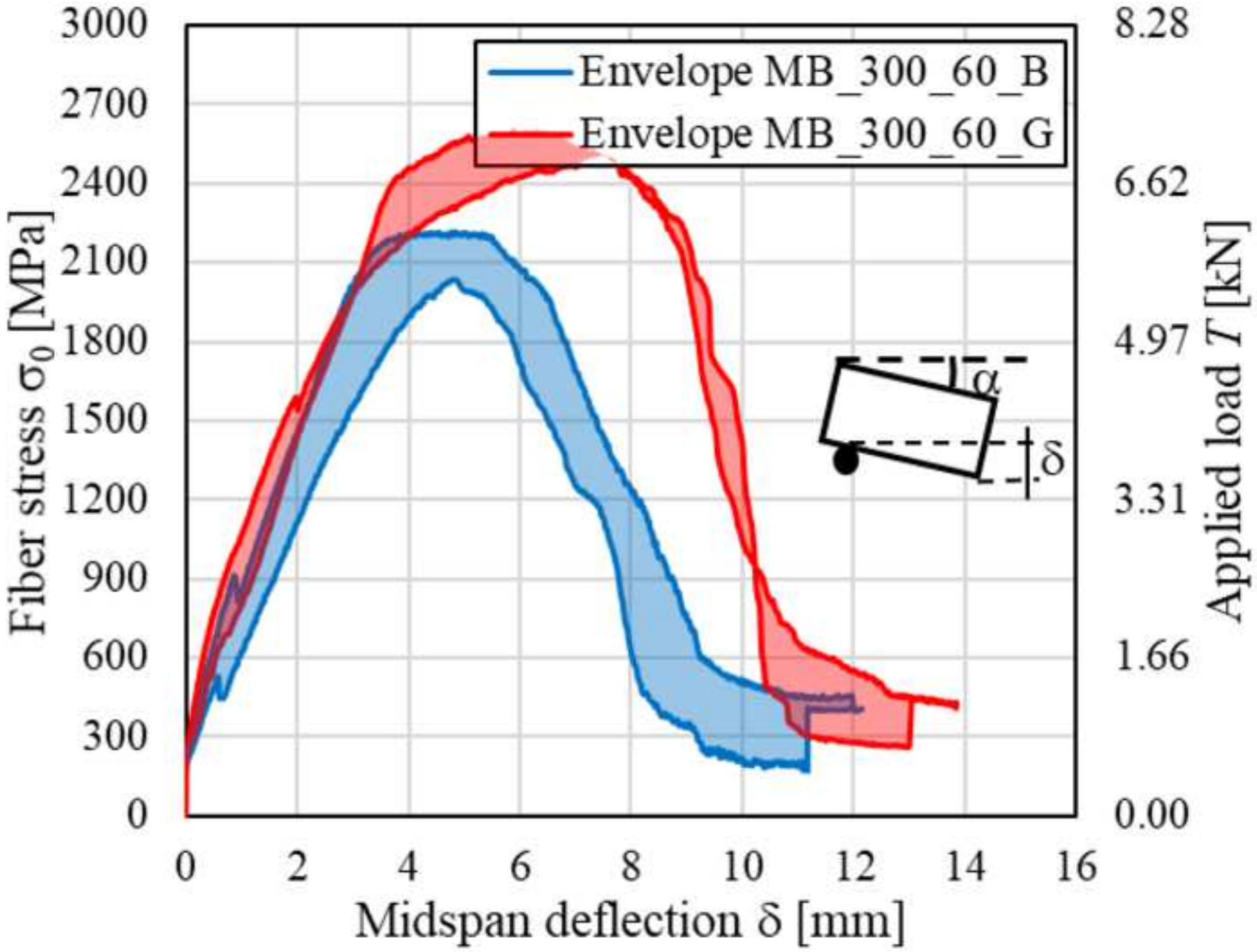

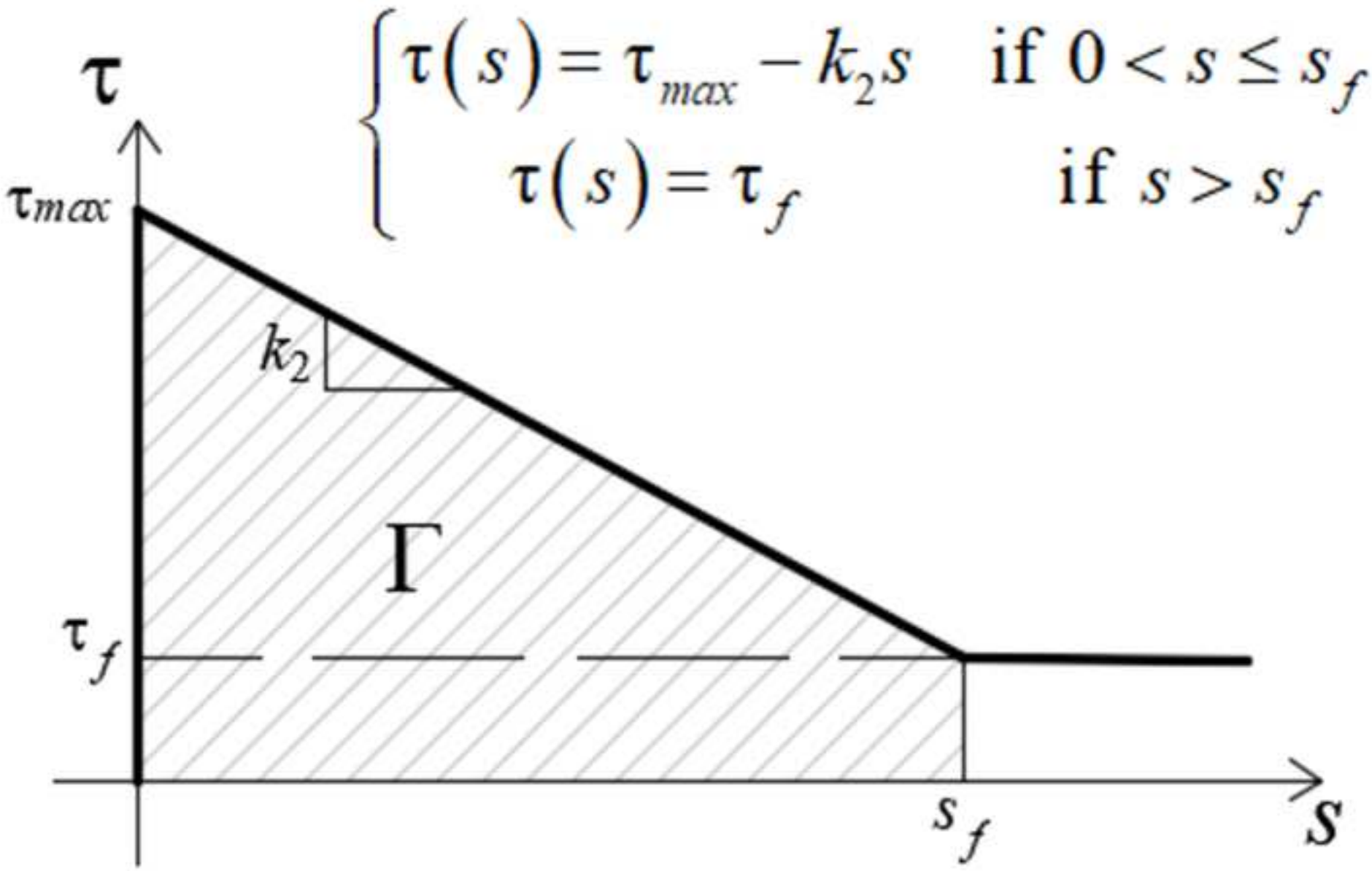

Figure_9

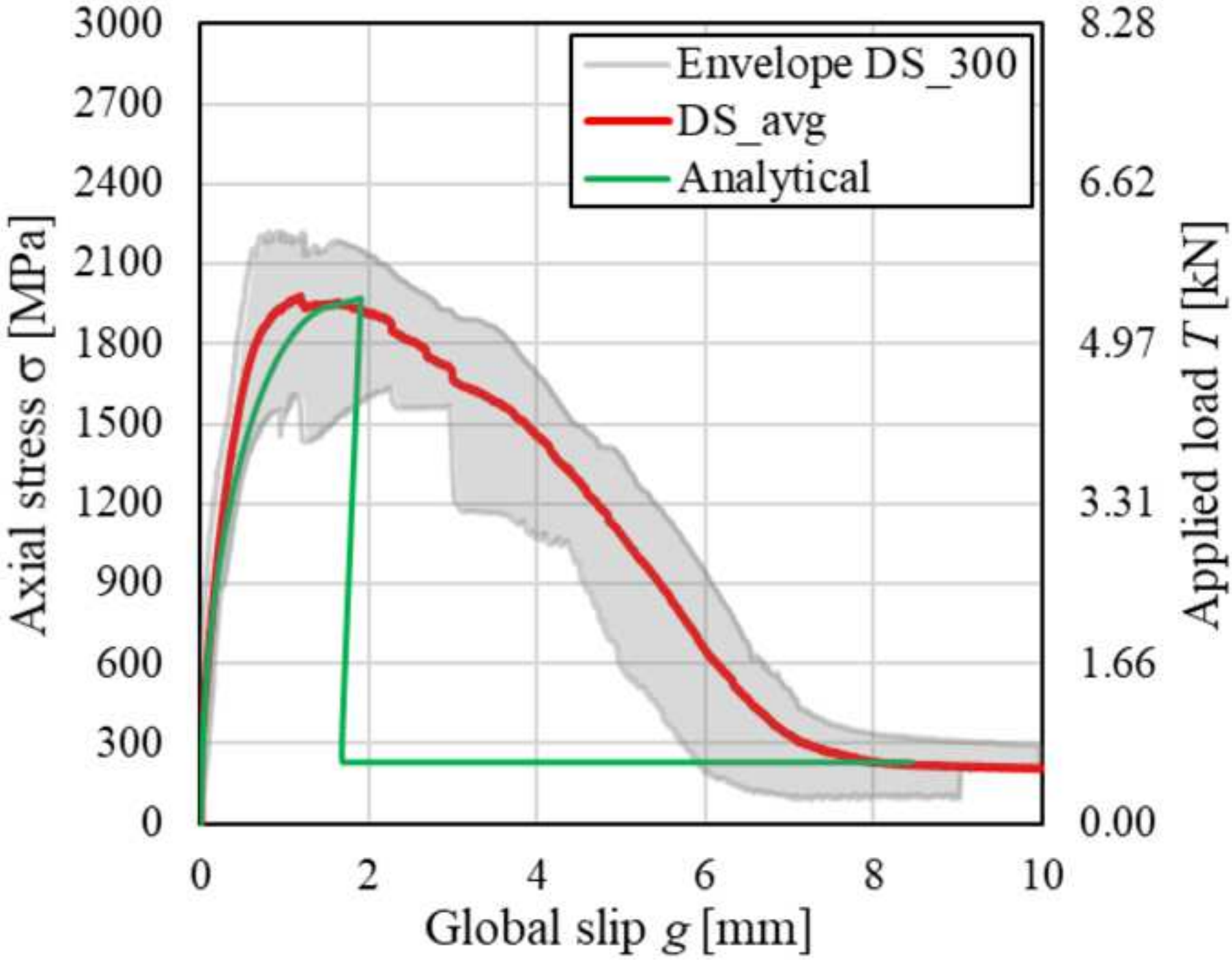

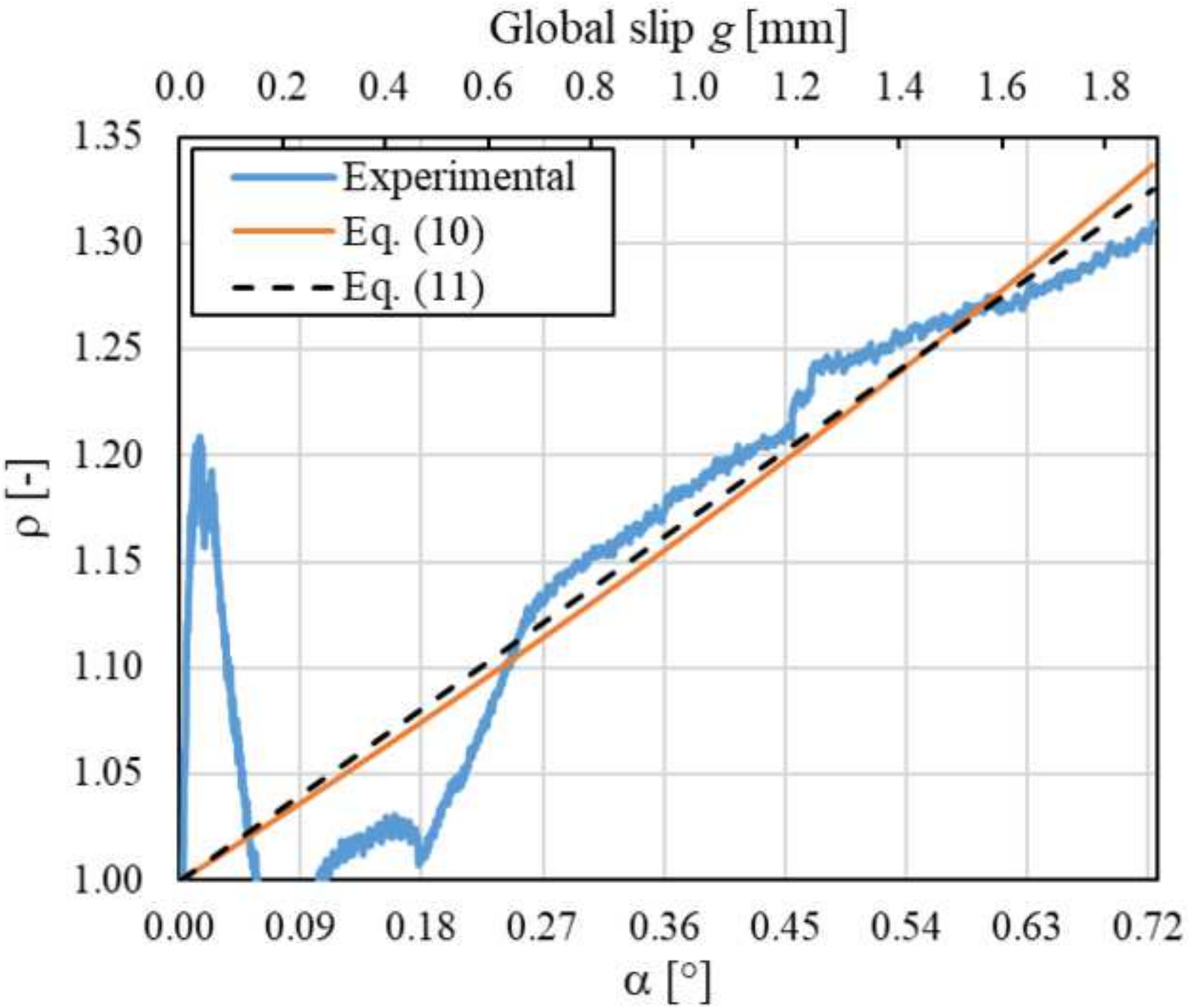

Figure_10b

Click here to access/download;Figure;Figure_10b.tiff

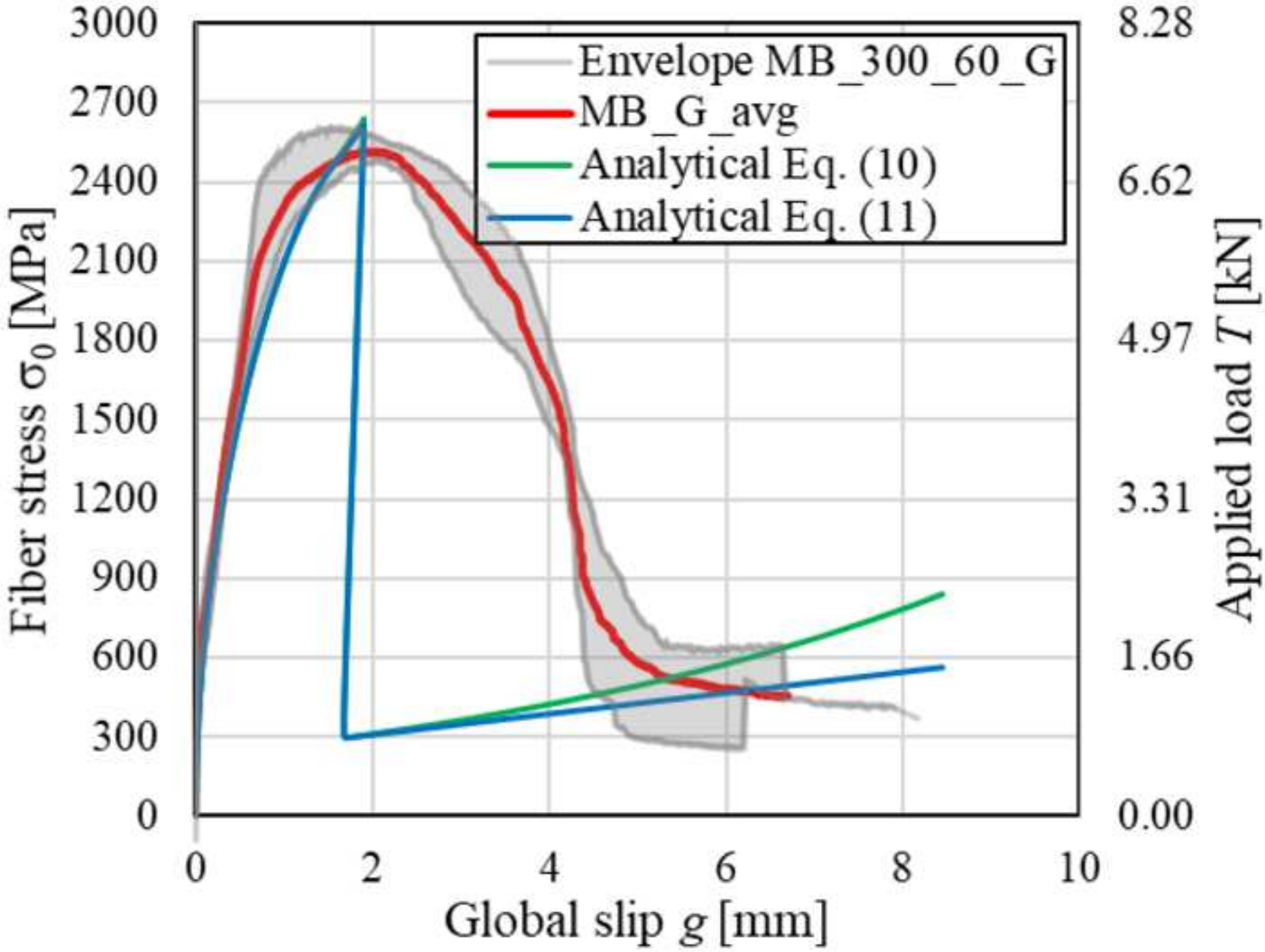

Figure-Table_3 Click here to access/download;Figure;Figure-Table_3.tiff

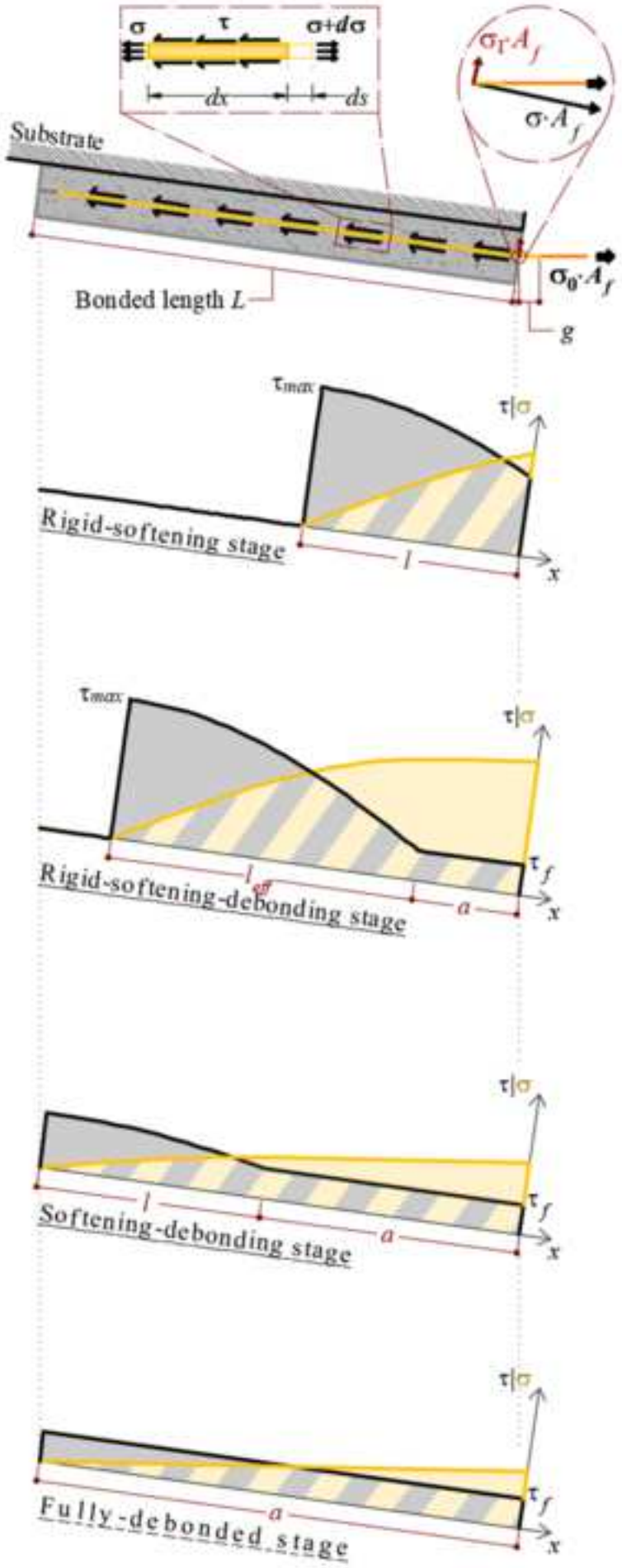

Conflict of Interest

The authors declare that there is no conflict of interest regarding the publication submitted.

CRediT author statement

Angelo Savio Calabrese: Conceptualization, Investigation, Data Curation, Writing - Original Draft.

Tommaso D'Antino: Conceptualization, Methodology, Validation, Writing- Reviewing and Editing.

Pierluigi Colombi: Supervision, Writing - Review & Editing, Funding acquisition.